

# DeepWEST: Deep Learning of Kinetic Models with the Weighted Ensemble Simulation Toolkit for Enhanced Sampling

Anupam Anand Ojha, Saumya Thakur, Surl-Hee Ahn, and Rommie E. Amaro\*



Cite This: *J. Chem. Theory Comput.* 2023, 19, 1342–1359



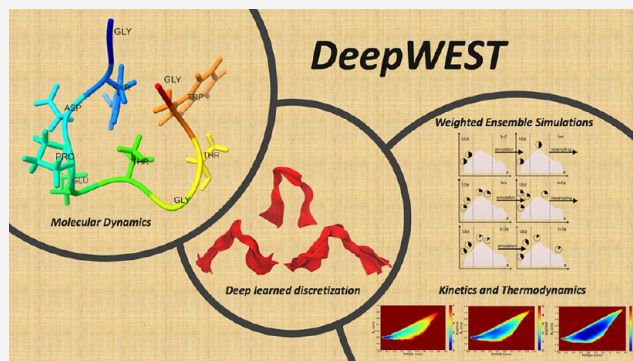
Read Online

ACCESS |

Metrics & More

Article Recommendations

**ABSTRACT:** Recent advances in computational power and algorithms have enabled molecular dynamics (MD) simulations to reach greater time scales. However, for observing conformational transitions associated with biomolecular processes, MD simulations still have limitations. Several enhanced sampling techniques seek to address this challenge, including the weighted ensemble (WE) method, which samples transitions between metastable states using many weighted trajectories to estimate kinetic rate constants. However, initial sampling of the potential energy surface has a significant impact on the performance of WE, i.e., convergence and efficiency. We therefore introduce deep-learned kinetic modeling approaches that extract statistically relevant information from short MD trajectories to provide a well-sampled initial state distribution for WE simulations. This hybrid approach overcomes any statistical bias to the system, as it runs short unbiased MD trajectories and identifies meaningful metastable states of the system. It is shown to provide a more refined free energy landscape closer to the steady state that could efficiently sample kinetic properties such as rate constants.



## 1. INTRODUCTION

Molecular dynamics (MD) simulations have found their applications in science and engineering, such as chemistry and biochemistry, statistical mechanics, condensed matter physics, and materials science.<sup>1–10</sup> In recent years, MD simulations have significantly impacted the study of complex biological processes such as protein folding, drug discovery, receptor–ligand binding and unbinding, protein–membrane interactions, and protein–protein interactions. MD simulations can effectively analyze key mechanistic insights into highly complex dynamics of biological systems of interest in atomistic detail.<sup>11–18</sup> However, the task of estimating the kinetics and thermodynamics of such systems comes with its own set of challenges.

Existing classical force fields are sometimes insufficient to estimate specific properties of interest, such as polarization and charge delocalization effects for complex biological systems.<sup>19–21</sup> Time steps for MD simulations are restricted to the femtosecond range to correctly integrate the equations of motion, as they cannot exceed the time period of the highest-frequency thermal oscillation. Biologically relevant systems undergo complex conformational transitions, which are essential to their functions. It is challenging to capture these transitions through conventional MD, especially if they are relatively slow processes (milliseconds or longer), involve large-scale conformational rearrangements, or include protein association and/or (re)folding. We resort to computationally

expensive long-scale MD simulations to observe such transitions or “rare events”.<sup>22–24</sup>

Several enhanced sampling methods have been developed to overcome the difference in time scales of conventional MD simulations compared to the time scales of biological processes.<sup>25–29</sup> One category of enhanced sampling methods adds a bias potential to the potential energy surface (PES) that decreases the energy barrier of transition between metastable states and accelerates the conformational search. We could roughly categorize these methods as collective variable (CV)-based and CV-free enhanced sampling methods. CV-based enhanced sampling approaches include but are not limited to metadynamics (metaD),<sup>30,31</sup> variationally enhanced sampling,<sup>32</sup> and Markov state models (MSMs),<sup>33,34</sup> while CV-free enhanced sampling methods include parallel tempering or replica exchange molecular dynamics (REMD),<sup>35,36</sup> selective integrated tempering, and Gaussian accelerated molecular dynamics (GaMD).<sup>37</sup> All of the previously mentioned enhanced sampling approaches are capable of accelerated

Received: March 21, 2022

Published: January 31, 2023



PES conformational search. Thereby, they prove to be effective in extensive thermodynamic sampling. On the contrary, such enhanced sampling approaches add a bias potential to the system's potential energy and thereby lead to altered dynamics. Extracting kinetic and mechanistic insights is often subjected to assumptions such as low residence times in the transition state regions, quasistationarity characteristics of metaD, construction of a master equation for non-Arrhenius and multistate kinetics, and usage of Kramers' rate theory in the overdamped regime.<sup>38–42</sup>

On the other hand, several path sampling methods exist for an extensive sampling of kinetic properties, which are broadly divided into complete path sampling and segment-based sampling. Transition path sampling (TPS) and dynamic importance sampling (DIMS) are based on complete reactant to product path sampling. Segment-based sampling approaches are based on splitting the reactant to product path into several segments or "bins" where bin-to-bin transitions are sampled by running independent MD simulations of fixed duration within these bins. These methods include but are not limited to weighted ensemble (WE) methodology,<sup>43</sup> milestoning approaches,<sup>44–46</sup> adaptive multilevel splitting (AMS),<sup>47–49</sup> and transition interface sampling (TIS).<sup>50</sup> These path sampling methods typically focus on sampling the transition regions, and thereby, an entire PES of the system is often neglected. The WE method enhances the sampling of rare events by running independent and unbiased parallel simulations in short configurational spaces or "bins". These simulations communicate with each other through replication and resampling, leading to the precise estimation of kinetic observables. The WE method is further explained in section 2.2.

Our recent work demonstrated the effectiveness of a hybrid enhanced sampling method, the GaMD-WE method, which combines GaMD and WE for an extensive sampling of both the thermodynamics and kinetics of biological systems of interest.<sup>51</sup> GaMD is performed initially to sample the PES of the system by applying several boost potentials and is followed by reweighting to recover the original PES. Configurations selected from the recovered PES are the starting structures for the WE simulations. Several independent boost potentials are applied in parallel GaMD simulations and are reweighted accordingly to recover the PES of the system. The GaMD run with the most PES coverage provides the starting structures for WE simulations. We aim to further decrease the computational cost of thermodynamic and kinetic sampling of systems of interest by running unbiased MD simulations and implementing deep learning with the Markovian variational approach for faster and enhanced hybrid sampling.<sup>52,53</sup> This way, we can bypass the entire reweighting process to recover the original PES.

Providing a well-sampled initial state distribution to WE simulations is often a concern. Generally, multiple starting structures are provided at the beginning of a simulation, and they often fail to establish extensive communication with each other, thereby leading to an initial bias in the simulation. MSMs have proved to be successful in generating equilibrium distributions, thereby removing the initial bias in the simulations.<sup>54</sup> The history-augmented Markov state model (haMSM) is another efficient method for the removal of bias in stationary distributions, and it has been implemented recently in WE simulations, where a steady-state analysis is performed, and the weights are distributed accordingly to restart the simulation.<sup>55</sup> In short, DeepWEST is an attempt to

construct MSMs from short MD simulations, providing a well-sampled initial distribution for the WE simulations. We propose a hybrid method that uses the variational approach for Markov processes (VAMP) and neural networks to identify metastable states from unbiased and short MD simulations as a precursor for running WE simulations. Selected conformations from these states then serve as starting structures for WE simulations to further sample the kinetics and thermodynamics of the system. This hybrid methodology further reduces the computational cost compared to our previously developed hybrid GaMD-WE method, accelerates the WE approach further by providing well-sampled initial configurations, and provides a better comprehensive picture of the thermodynamic and kinetic properties of the systems of interest by introducing no statistical bias into the free energy landscape of the system. In the forthcoming sections, we will describe the WE method, the VAMP approach, and the hybrid method in detail. We will also demonstrate the capability of the DeepWEST approach to sample kinetic and thermodynamic properties faster than the WE method alone and compare the findings with those of the already established GaMD-WE approach.

## 2. METHODS

### 2.1. Variational Approaches for Markovian Processes.

Markovian processes are stochastic processes where the future state of the system,  $\mathbf{x}_{t+\tau}$  depends only on the current state,  $\mathbf{x}_t$ , where  $t$  is the time step and  $\tau$  is the lag time. Various Markov modeling approaches have been developed recently to extract key information for complex dynamical processes. These methods include but are not limited to Markov state models (MSMs),<sup>56–58</sup> Markov transition models, variational approach to conformational dynamics (VAC),<sup>59</sup> time-lagged independent component analysis (TICA),<sup>60</sup> variational diffusion maps,<sup>61,62</sup> and variational approach for Markov processes (VAMP).<sup>52,63</sup> Dynamical systems often display high nonlinearity in their system coordinates. To analyze nonlinear and high-dimensional dynamical systems, we employ the Koopman operator,  $\mathbb{K}$ , that linearly transforms the vector space spanned by observables in the form of time-series data generated by MD simulations. This facilitates the prediction and estimation of nonlinear dynamical properties through the traditional methods employed for linear dynamical systems.<sup>64–66</sup> A majority of the Markovian modeling approaches exploit the fact that there exists a nonlinear transformation of these features such that the dynamics can be approximated as a linear Markov model.<sup>67,68</sup> Let  $\chi_0$  and  $\chi_1$  be the feature transformations for the trajectory coordinates  $\mathbf{x}_t$  and  $\mathbf{x}_{t+\tau}$  respectively, and  $\mathbb{E}$  be the expectation value such that the matrix  $\mathbb{K}$  determines the dynamics of the system according to eq 1:

$$\mathbb{E}[\chi_1(\mathbf{x}_{t+\tau})] \approx \mathbb{K}^T \mathbb{E}[\chi_0(\mathbf{x}_t)] \quad (1)$$

According to the VAMP theory, when the subspaces spanned by the features,  $\chi_0$  and  $\chi_1$ , are identical to the top left and top right singular functions of  $\mathbb{K}$ , we obtain the best finite-dimensional linear model.

To generate well-sampled initial conformations for WE simulations, we resort to a neural network architecture that employs VAMP, known as VAMPnets, which is a nonbiased trajectory learning approach towards faster estimation of kinetics and thermodynamics of systems of interest compared to other hybrid approaches.<sup>69</sup> MD data analysis is primarily

performed in subsequent steps of featurization, dimension reduction, discretization, and coarse-graining.<sup>70–73</sup> Featurization is the process where the simulation data are often subjected to the removal of translational and rotational motion and/or transformed into internal coordinates. Featurization follows a dimensionality reduction where high-dimensional trajectory data are reduced to slow collective variables.<sup>74–76</sup> However, initial steps of featurization, such as choosing appropriate metrics for training the trajectory dataset such as using Cartesian coordinates or internal coordinates, selecting suitable CVs that describe the conformation space such as dihedral angle root-mean-square deviation (RMSD), radius of gyration, removal of solvent coordinates, selection of heavy atoms, and realignment, are to be determined before training the trajectory using VAMPnets. The resultant metric space is then discretized to fewer states, and the process is called discretization.<sup>71,77,78</sup> Finally, coarse-graining of the MSM is performed since the internal dynamics of a particular set of microstates can be faster than the modeling time scale.<sup>79,80</sup> All of the above steps involved in the process of generating MSMs are performed by VAMPnets that learn the nonlinear collective variables or reaction coordinates that separate the metastable states of biological systems.

A simple VAMPnets model comprises two parallel neural network architectures that are employed to learn feature transformations using the VAMP approach. Each network receives the initial MD trajectory coordinates,  $\mathbf{x}_0$ , and time-lagged correspondent of the same coordinates,  $\mathbf{x}_{t+\tau}$ . Nonlinear dimensionality reduction is then performed on these two sets of trajectory inputs for each time step,  $t$ . As per the VAMP principle, a VAMP-2 score is defined that attains its maximum value when the top left and top right components of the Koopman operator  $\mathbb{K}$  are equivalent to the subspaces spanned by these features.<sup>52</sup> Deployed neural networks are trained to maximize the VAMP-2 score in order to achieve the best finite-dimensional linear model. In the above process, it achieves the segregation of the trajectory frames and assigns them to particular clusters or Markov states, which then accelerates the process of rare-event sampling and transition state analysis. Key features for VAMPnets include the choice of the lag time, the number of output nodes, and the network depth of the architecture. A few preoptimization runs with varying lag times are performed on the simulation trajectory to find the lag time that could resolve the slowest processes. The choice of a lag time relies upon the eigenvalue decomposition of the Markov propagators. When selecting a large lag time that exceeds the time scale of the slowest processes, it becomes difficult to fit the noisy data. However, a short lag time leads to them getting stuck in one of the suboptimal maxima of the training score. The selection of output nodes represent the separable metastable regions from the trajectory data. A higher number of output nodes may not be suitable for small amounts of trajectory data since the clustering will lead to discretization of the transition regions. The clustering of metastable states also depends heavily on the network depth of the architecture. A deeper network describes complex functions and is more difficult to train.

**2.2. Weighted Ensemble Method.** Standard unbiased MD simulations are limited by the time scale and infrequency of significant biological events. Such events are rarely captured in the trajectory data, and it becomes challenging to analyze further and estimate the kinetics of such transitions. The weighted ensemble simulation approach is an enhanced

sampling method designed to sample such rare occurrences or transitions such as protein–protein association reactions and conformational changes by replicating and resampling an ensemble of weighted trajectories.<sup>43,81</sup> The whole configurational space is subdivided into macrostates or “bins” that sequentially lead the system from an initial state to the target state. Many short simulations or “walkers” carrying probabilities or “weights” are run, and the system evolves throughout the simulation through “resampling” that ensures an equal number of trajectories in each bin, i.e., by splitting or merging walkers. These walkers explore the configurational space extensively, eventually sampling rare transitions. Appropriate progress coordinates are used to define the bin boundaries. Transitions between these bins are recorded while the system evolves in time to estimate the kinetics and thermodynamics. The WE method has been demonstrated to accurately estimate the kinetics of rare events for multiple biological systems.<sup>82,83</sup>

Resampling is a crucial component of the WE approach that leads to the statistically unbiased future evolution of the system.<sup>82,84,85</sup> Walkers are resampled after every iteration via appropriate replication and reassignment of weights. Weighted trajectories are initiated from assigned bins and are propagated for a short interval,  $\tau$ . These trajectories are either replicated where there are too few trajectories or deleted where there are more than the required number of trajectories per bin. Since there is no statistical bias in the simulation, thermodynamic and kinetic properties can be directly obtained by evolution of the weights of the walkers in each bin. Simulation results can be periodically checked for convergence by estimating rate constants for various possible transitions between the macrostates. This approach also eliminates the need for choosing the resampling time,  $\tau$ , based on the Markovian property and thereby provides the flexibility to select  $\tau$  based on the system size.

The efficiency of WE simulations is attributed to the weights of the starting conformations, and long-scale simulations of multiple short trajectories are required to obtain accurate kinetic and thermodynamic properties of systems of interest. The choice of initial starting conformations significantly affects the accuracy and simulation time, and it can be remarkably enhanced by providing an intelligently sampled set of initial starting conformations. The motivation for DeepWEST originates from this notion and aims at obtaining these conformations through deep learning approaches using VAMP. The Weighted Ensemble Simulation Toolkit with Parallelization and Analysis (WESTPA) is an open-source package to perform WE simulations.<sup>86</sup> This toolkit is highly interoperable, is compatible with a wide range of MD engines, and provides an integrated protocol for efficient storage and analysis of the estimates generated. Our current work incorporates the WESTPA package for running WE simulations. Since we are focused on obtaining the rate constants between multiple states in these systems, we run equilibrium WE simulations to sample their kinetic and thermodynamic properties. However, steady-state WE simulations can be employed for systems where rate constants between two states are calculated. Such simulations employ “target state recycling”, i.e., the walkers are fed into the initial state once they reach the target state. Steady-state WE simulations with starting states from equilibrium WE are more commonly used for sampling kinetic and thermodynamic properties.

**2.3. DeepWEST.** The deep learning of kinetic models with the Weighted Ensemble Simulation Toolkit (DeepWEST)



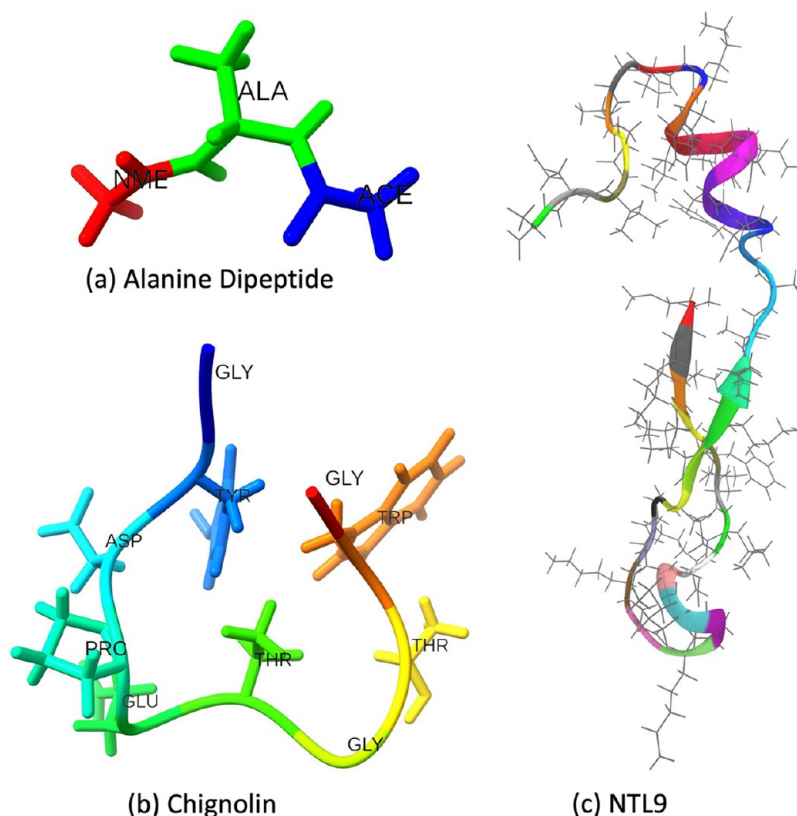


**Figure 1.** Model systems tested by the WE, GaMD-WE, and DeepWEST approaches.

method aims to provide well-sampled initial distributions to WE simulations. It is achieved by running a relatively short MD simulation and processing the trajectory data through the VAMP approach by employing neural networks. Initial conformations for WE simulations and their probabilistic values are extracted from the resultant MSMs. WE simulations are then run with this distribution, generating a more refined free energy landscape closer to the steady-state distribution. We have developed a DeepWEST package that automates the entire process of running MD simulations for trajectory analysis, performing deep learning of kinetic models for generating MSMs through VAMPnets, and producing well-sampled initial conformations for running WE simulations. The entire workflow can be described as follows:

1. Systems of interest are downloaded from the Protein Data Bank (PDB) server and are prepared for MD simulations using appropriate force field parameters, periodic box vectors, and solvation using the Amber 14 package.<sup>87</sup>
2. Once the system is prepared, energy minimization, simulated heating, and equilibration are performed using the OpenMM simulation engine.<sup>88</sup>
3. The MD simulation is then performed using the Amber simulation engine for the desired amount of simulation time. Trajectories are saved with the desired frequency.
4. The trajectory data are subjected to featurization, dimensionality reduction, discretization, and kinetic modeling using VAMPnets to generate metastable states.
5. VAMPnets deploy a “fuzzy clustering” of MD trajectories in “ $n$ ” output states. Each conformation in the MD trajectory has a probability for each of these output states that sum to 1. The cluster with the

maximum likelihood for each conformation is the one that is assigned to the conformation. After clustering, conformations within each cluster are further binned based on one of the CVs (dihedral angle,  $\phi$ , in the case of alanine dipeptide and RMSD in the case of chignolin). From each subcluster, a certain number of conformations are selected from each bin to generate a well-sampled initial state sampling for WE simulations. Once the conformations are chosen from these clusters, they are assigned weights based on the fractions of the population of the clusters to which they belong.

6. A WE simulation folder is created with all of the required starting structures, weights, and topology files to run a WE simulation. To avoid any steric clashes during the initial WE simulations, starting structures are processed in subsequent steps of minimization of heavy atoms (N, C, O, and  $C_{\alpha}$ ) followed by minimization of the entire system.
7. WE simulations are then run with the starting structures with desired probabilities assigned for each conformation.

As shown in **Results**, our method estimates the kinetics of the systems of interest, i.e., alanine dipeptide and chignolin, more quickly and more accurately than the WE method alone. Long-scale unbiased MD simulations or brute-force methods are often used as a reference for evaluating the performances of new methods on model systems.<sup>89</sup> Five independent brute-force simulations, each 2  $\mu$ s for alanine dipeptide and 4  $\mu$ s for chignolin, were performed to obtain the reference values of rate constants over aggregate simulation time. DeepWEST performs equally well and often surpasses the brute-force and hybrid GAMD-WE approaches with the advantage of being

computationally inexpensive and easy to implement while adding no statistical bias to the system.

### 3. RESULTS

To demonstrate the effectiveness of the current approach, we have tested the DeepWEST method on three systems: alanine dipeptide with explicit solvation (Figure 1a), chignolin with implicit solvation (Figure 1b), and the NTL9 protein with implicit solvation (Figure 1c). Kinetics and thermodynamics obtained from these systems using our DeepWEST approach are compared with those obtained using WE and our previously developed hybrid GaMD-WE approach. For the systems mentioned above, we demonstrate that the DeepWEST approach surpasses the WE approach in estimating the rate constants between the metastable states of interest and even outperforms the already established hybrid GaMD-WE approach in many occurrences. We also demonstrate that DeepWEST samples the free energy landscape equivalently compared to the already established approaches. Error bars representing 95% confidence intervals are calculated for all WE, GaMD-WE, and DeepWEST runs. Simulations are run until there is no significant change in the average rate constant or “convergence” is reached. Rate constants are plotted with an approximate interval of 50 iterations for each run.

**3.1. Alanine Dipeptide.** Alanine dipeptide has been commonly used as a model system for testing new methods.<sup>13,51,90–92</sup> It is a 22-atom system with an acetyl group at the N-terminus and N-methylamide at the C-terminus (Figure 1a). Initial coordinates for alanine dipeptide were obtained from <http://ftp.imp.fu-berlin.de/pub/cmb-data/alanine-dipeptide-nowater.pdb>. The AMBER ff14SB force field was used to prepare the system for MD simulations.<sup>93</sup> It was then subjected to explicit solvation using the TIP3P water model.<sup>94</sup> Alanine dipeptide was subjected to 50 ns of unbiased MD simulations. Trajectories were trained using VAMP neural networks with a time lag of 80 ps, a training ratio of 0.9, and a batch size of 1000 that learned discretization in three metastable states. A list of hyperparameters used for network training is provided in Table 1. Starting structures

**Table 1. Hyperparameters Used in VAMPNets for Alanine Dipeptide**

hyperparameter	description	value
$\tau$	time lag between the two MD trajectory datasets	80 ps
batch size	number of samples in a batch for gradient descent	1000
train ratio	percentage of trajectory points used for training	0.9
network depth	number of hidden layers in the network	8
layer width	width of the hidden layer	100
learning rate	learning rate used for the ADAM optimizer	$1 \times 10^{-4}$
output size	number of metastable states as an output	3
$n_{\text{epochs}}$	number of iterations over the training set	100
$\epsilon$	threshold for eigenvalues	$1 \times 10^{-5}$

were selected from the metastable states as per the DeepWEST protocol, followed by three independent WE simulations of 12  $\mu\text{s}$  each with a total simulation time of 36  $\mu\text{s}$ . The resampling time,  $\tau$ , was identical to that used in the WE and GaMD-WE runs, i.e., 10 ps.<sup>51,82</sup> CVs were set to be the dihedral angles,  $\phi$  and  $\psi$ , which were evenly spaced in bins of 0.17 rad with  $\phi$  and

$\psi$  in the range  $[-3.14 \text{ rad}, 3.14 \text{ rad}]$ . The target number of walkers per bin,  $n_w$ , was set to be 4 for the WE simulation.

To compare the performance of the DeepWEST method with the WE and hybrid GaMD-WE methods, we have identified three metastable states in alanine dipeptide as shown in Figure 2a. Note that Figure 2b shows the three metastable states when the simulation time was 250 ns. For the DeepWEST method, we have used the 50 ns simulation time as an input trajectory to be trained by the network architecture. The metastable states were chosen in such a way that each state represents an important region of the PES. These regions are  $\alpha_R$ ,  $\alpha_L$ , and  $P_{II}$ .  $\alpha_R$  lies within the  $\alpha$  region of the Ramachandran plot, while  $P_{II}$  lies in the  $\beta$  region (Figures 2 and 3).  $\alpha_L$  lies in the region where  $\phi$  attains positive radian values.  $\alpha_R$  is defined as  $-2.09 \text{ rad} \leq \phi \leq 0 \text{ rad}$  and  $-1.75 \text{ rad} \leq \psi \leq 0.87 \text{ rad}$ , and  $\alpha_L$  is defined as  $0 \text{ rad} \leq \phi \leq 2.09 \text{ rad}$  and  $-0.87 \text{ rad} \leq \psi \leq 1.75 \text{ rad}$ ;  $P_{II}$  is defined as  $-2.09 \text{ rad} \leq \phi \leq 0 \text{ rad}$  and  $1.31 \text{ rad} \leq \psi \leq 3.14 \text{ rad}$ . VAMPNets demonstrated success in discretization of the MD trajectory data in three metastable states separating the  $\alpha$  and  $\beta$  regions of the Ramachandran plot (Figure 2a) and further separating the conformations with the negative and positive values of the  $\phi$  angles (Figure 2b).

Two different WE approaches, namely, the conventional WE approach and the hybrid GaMD-WE approach, were compared to assess the performance of our newly developed DeepWEST approach. WE was run for a total simulation time of 36  $\mu\text{s}$  averaged over three independent runs of 12  $\mu\text{s}$  each. Similarly, the GaMD-WE approach was run for 50 ns of GaMD followed by 11.95  $\mu\text{s}$  of WE, totaling a simulation time of 36  $\mu\text{s}$  averaged over three independent runs of 12  $\mu\text{s}$  each. Likewise, the DeepWEST approach was run for an unbiased MD simulation of 50 ns followed by 11.95  $\mu\text{s}$  of WE simulation, totaling a simulation time of 36  $\mu\text{s}$  averaged over three independent runs of 12  $\mu\text{s}$  each. Figure 2 demonstrates the ability of the deep-learned kinetic modeling approach to cluster the MSMs and also to ensure that adequate sampling has been achieved to select starting conformations. The average free energy is given by  $-k_B T \ln P$ , where  $k_B$  is the Boltzmann constant,  $T$  is the absolute temperature, and  $P$  is the probability. Figure 4a,b presents the average free energy profiles of alanine dipeptide for the WE and hybrid GaMD-WE approaches, respectively, while Figure 4c represents the free energy profile for the DeepWEST approach. Figure 4c shows almost identical PES coverages obtained through the DeepWEST approach compared to WE (Figure 4a) and the hybrid GaMD-WE approach (Figure 4b). This in turn demonstrates the ability of the DeepWEST approach to access the entire free energy landscape of the system with enough sampling in the  $P_{II}$ ,  $\alpha_L$ , and  $\alpha_R$  (right-handed  $\alpha$ -helix) regions. Figure 5 demonstrates the average free energy profiles of alanine dipeptide from three separate runs of WE, GaMD-WE, and DeepWEST simulations at different stages of the simulations.

To explore the performance of the DeepWEST approach in estimating kinetic rates, brute-force simulations were carried out to obtain reference values. Three independent 12  $\mu\text{s}$  simulations were run, and Bayesian bootstrapping was performed for 95% confidence intervals. Rate constants were obtained from different methods, i.e., the brute-force calculations and the WE, GaMD-WE, and DeepWEST methods, for transitions between metastable regions of interest (Table 2). For the transitions between the central metastable region,  $\alpha_R$  to  $P_{II}$ , the DeepWEST method outperformed both

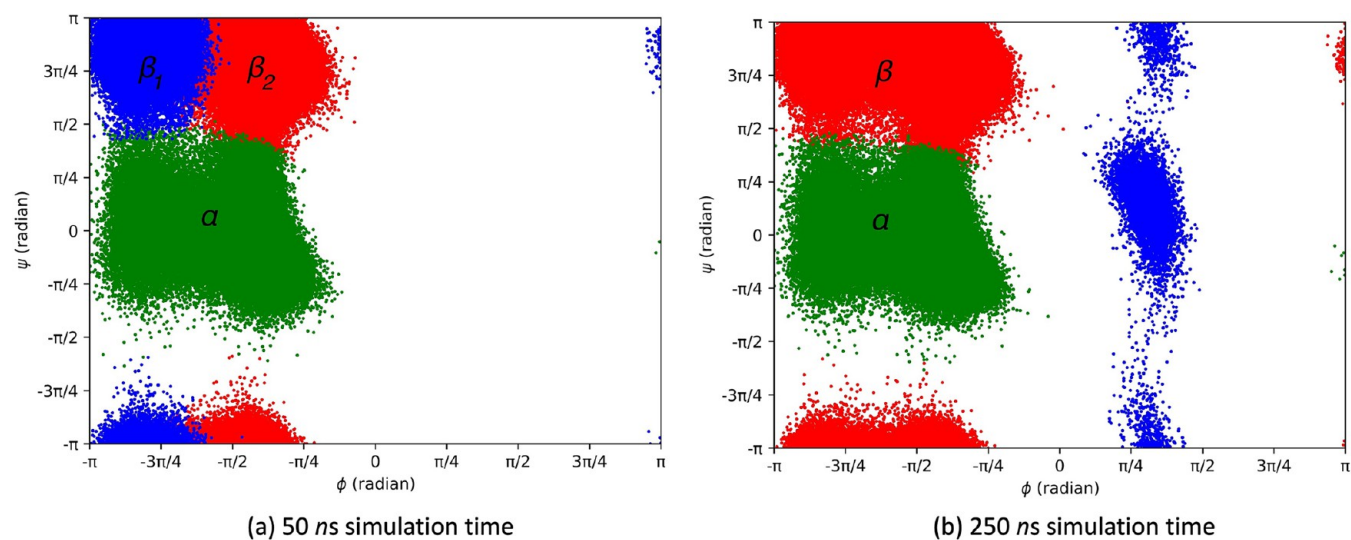


**Figure 2.** Three metastable states of alanine dipeptide as an output of VAMPNets (a) separated by  $\alpha$  (green) and  $\beta$  (red and blue) regions of the Ramachandran plot and (b) separated by negative (green and red) and positive (blue) values of  $\phi$  and further separated by  $\alpha$  (green) and  $\beta$  (red) regions of the Ramachandran plot.

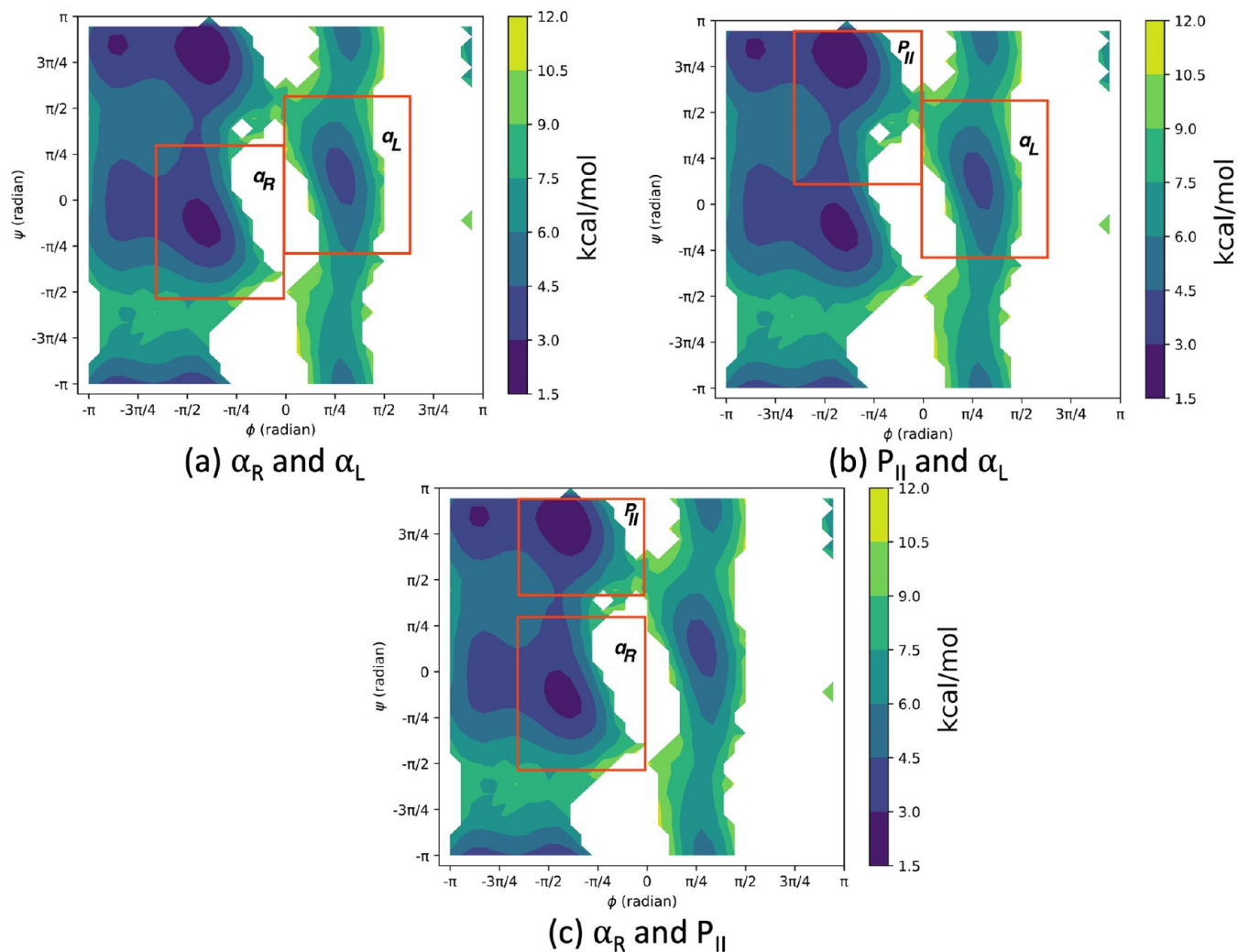


**Figure 3.** Average free energy profiles of alanine dipeptide from three separate 12  $\mu$ s DeepWEST simulations. Rate constants to be calculated between the following regions of interest in alanine dipeptide: (a)  $\alpha_R \leftrightarrow \alpha_L$ ; (b)  $P_{II} \leftrightarrow \alpha_L$ ; (c)  $\alpha_R \leftrightarrow P_{II}$ .



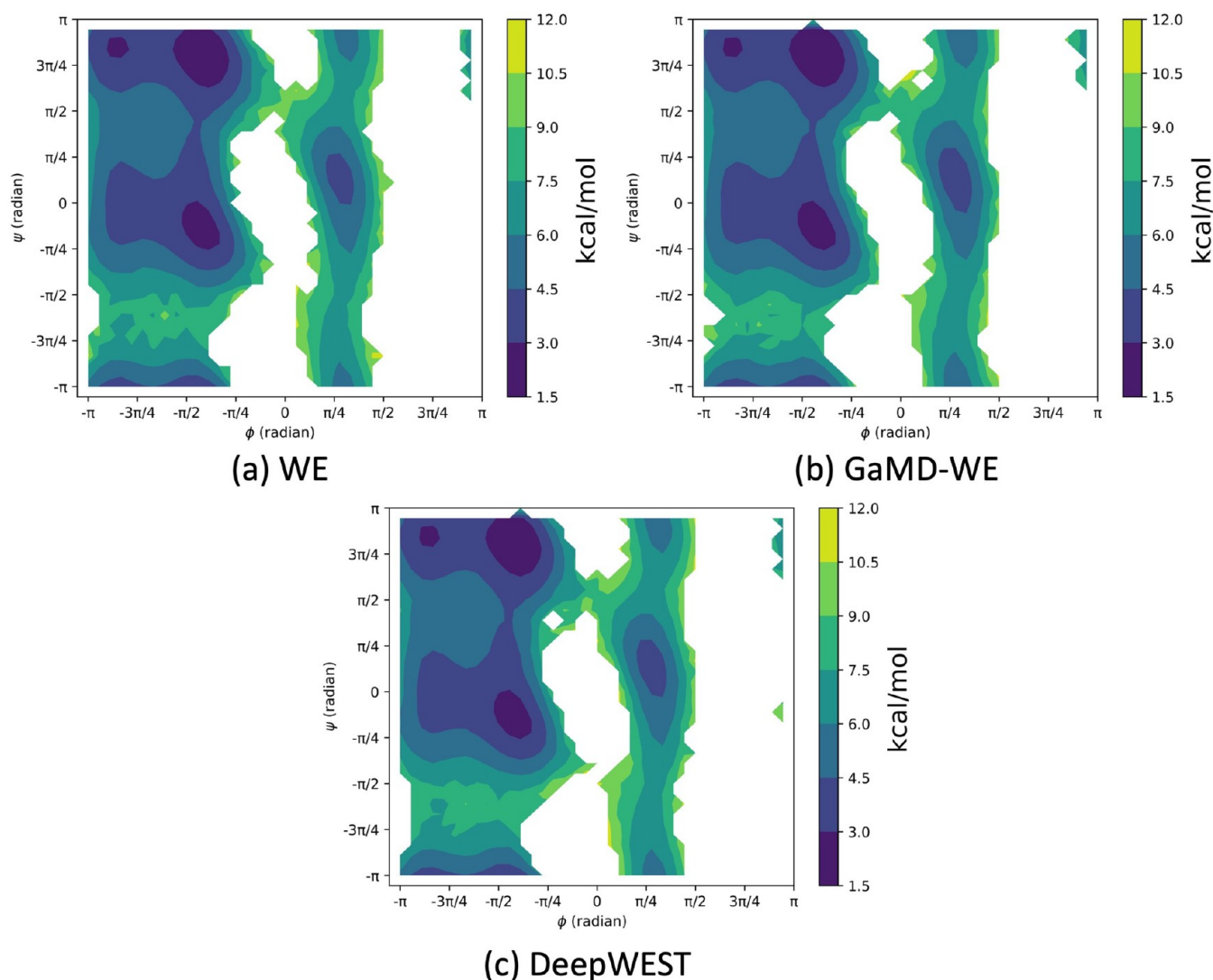


**Figure 4.** Average free energy profiles of alanine dipeptide from three separate 12  $\mu$ s runs of (a) WE, (b) GaMD-WE, and (c) DeepWEST simulations.

the WE and GaMD-WE methods in estimating the rate constant. The rate constant for the DeepWEST method converged faster compared to the brute-force value (Figure 6c). However, as observed in Figure 6d, all of the methods slightly overestimated the rate constant for the transition from  $P_{II}$  to  $\alpha_R$ . In the transitions from  $\alpha_L$  to  $P_{II}$  (Figure 6a),  $P_{II}$  to  $\alpha_L$  (Figure 6b),  $\alpha_R$  to  $\alpha_L$  (Figure 6e), and  $\alpha_L$  to  $\alpha_R$  (Figure 6f), comparable convergence and accuracy of the kinetic rates were observed for the DeepWEST approach compared to the WE and GaMD-WE methods.

**3.2. Chignolin.** Chignolin (PDB ID 1UAO), a designed protein, is a model system consisting of 10 amino acid residues (GYDPETGTWG) (Figure 1b).<sup>95</sup> It forms a stable  $\beta$ -hairpin structure in implicit solvent, and MD simulations reveal the slow unfolding of chignolin.<sup>96</sup> Initial coordinates for chignolin were obtained from <https://files.rcsb.org/download/1UAO.pdb>. The system was then subjected to generalized Born (GB) implicit solvation using the model II radii.<sup>97–99</sup> The AMBER ff14SB force field was used to prepare the system for MD simulations.<sup>93</sup> Chignolin was subjected to 100 ns of constant-volume unbiased MD simulation with a collision frequency of 1  $\text{ps}^{-1}$ , employing a Langevin thermostat at a constant

temperature of 300 K. To interpret the kinetics of a system that demonstrates folding and unfolding behavior, we encounter the problem of trajectory alignment with respect to a unique reference structure. Moreover, a large amount of noise would be introduced while the networks transform the data via rotations and translations. Hence, for the chignolin system, internal coordinates were chosen as a network input. Nearest-neighbor heavy-atom distances between all non-redundant residues separated by two or more residues served as the network input, resulting in 28 nodes. MD trajectories were trained using VAMP neural networks with a time lag of 40 ps, a training ratio of 0.9, and a batch size of 1000 that learned discretization in three metastable states by performing a hierarchical decomposition of the state space. A list of hyperparameters used for network training is provided in Table 3. Starting structures were selected from the metastable states as per the DeepWEST protocol, followed by three independent WE simulations of 40  $\mu$ s each with a total simulation time of 120  $\mu$ s. The resampling time,  $\tau$ , was identical to that used in the WE and GaMD-WE runs, i.e., 20 ps.<sup>51</sup> CVs for WE simulations were set to be mass-weighted RMSD and mass-weighted radius of gyration ( $R_g$ ), respectively. Both CVs were

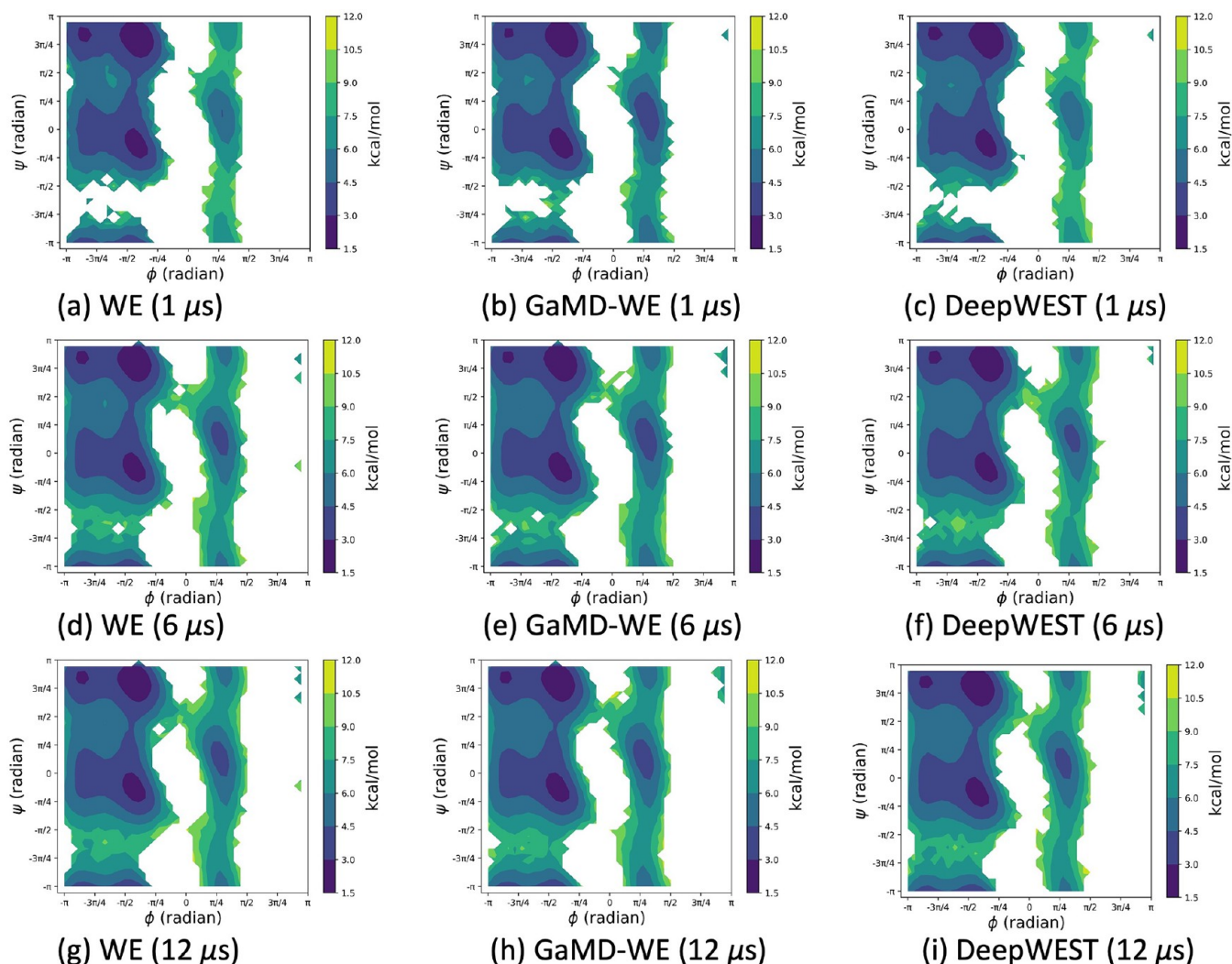


**Figure 5.** Average free energy profiles of alanine dipeptide from three separate runs of WE, GaMD-WE, and DeepWEST simulations at different stages of the simulations.

**Table 2.** Rate Constants (in  $\text{ns}^{-1}$ ) between Different Metastable States of Alanine Dipeptide Obtained after 12  $\mu$ s of Aggregate Simulation Time

transition	brute-force <sup>a</sup>	WE <sup>b</sup>	GaMD-WE <sup>b</sup>	DeepWEST <sup>b</sup>
$\alpha_L \rightarrow P_{II}$	0.335 [0.275, 0.408]	$0.325 \pm 0.022$	$0.328 \pm 0.012$	$0.336 \pm 0.015$
$P_{II} \rightarrow \alpha_L$	0.01 [0.008, 0.012]	$0.009 \pm 0.002$	$0.008 \pm 0.001$	$0.009 \pm 0.001$
$\alpha_R \rightarrow P_{II}$	6.812 [6.723, 6.897]	$6.971 \pm 0.046$	$6.737 \pm 0.037$	$6.788 \pm 0.155$
$P_{II} \rightarrow \alpha_R$	2.823 [2.777, 2.868]	$3.012 \pm 0.052$	$2.941 \pm 0.042$	$2.975 \pm 0.024$
$\alpha_R \rightarrow \alpha_L$	0.01 [0.008, 0.012]	$0.009 \pm 0.002$	$0.008 \pm 0.002$	$0.009 \pm 0.001$
$\alpha_L \rightarrow \alpha_R$	0.305 [0.254, 0.367]	$0.375 \pm 0.27$	$0.325 \pm 0.073$	$0.445 \pm 0.427$

<sup>a</sup>In the case of the brute-force simulation, the first value indicates the average rate constant, and the values within the brackets indicate the 95% confidence interval computed using Bayesian bootstrapping. <sup>b</sup>For the WE, GaMD-WE, and DeepWEST methods, the error bars represent 95% confidence intervals obtained from the standard deviations of three independent runs.

evenly spaced in bins of 0.02 nm in the range [0 nm, 1 nm]. The target number of walkers per bin,  $n_w$ , was set to 4 for the WE simulation.

To compare the performance of the DeepWEST method with the hybrid GaMD-WE and WE methods, we have identified three metastable states in chignolin as shown in Figure 7. These regions are folded, unfolded, intermediate I ( $I_1$ ), and intermediate II ( $I_2$ ). The folded region is defined as  $\text{RMSD} \leq 0.20$  nm, while the unfolded region is defined as  $\text{RMSD} \geq 0.55$  nm.  $I_1$  is defined to be  $0.20 \text{ nm} \leq \text{RMSD} \leq 0.30$

nm and  $0.425 \text{ nm} \leq R_g \leq 0.525$  nm, while  $I_2$  is defined to be  $0.60 \text{ nm} \leq \text{RMSD} \leq 0.70$  nm and  $0.70 \text{ nm} \leq R_g \leq 0.80$  nm.

Chignolin represents a common protein structural motif that undergoes folding and unfolding during brute-force MD simulations. We tested the DeepWEST method by estimating rate constants between regions of interest, especially in the folded and unfolded regions. WE was run for a total simulation time of 120  $\mu$ s averaged over three independent runs of 40  $\mu$ s each. Similarly, for the GaMD-WE approach, six independent 500 ns runs of GaMD were performed with varying boost



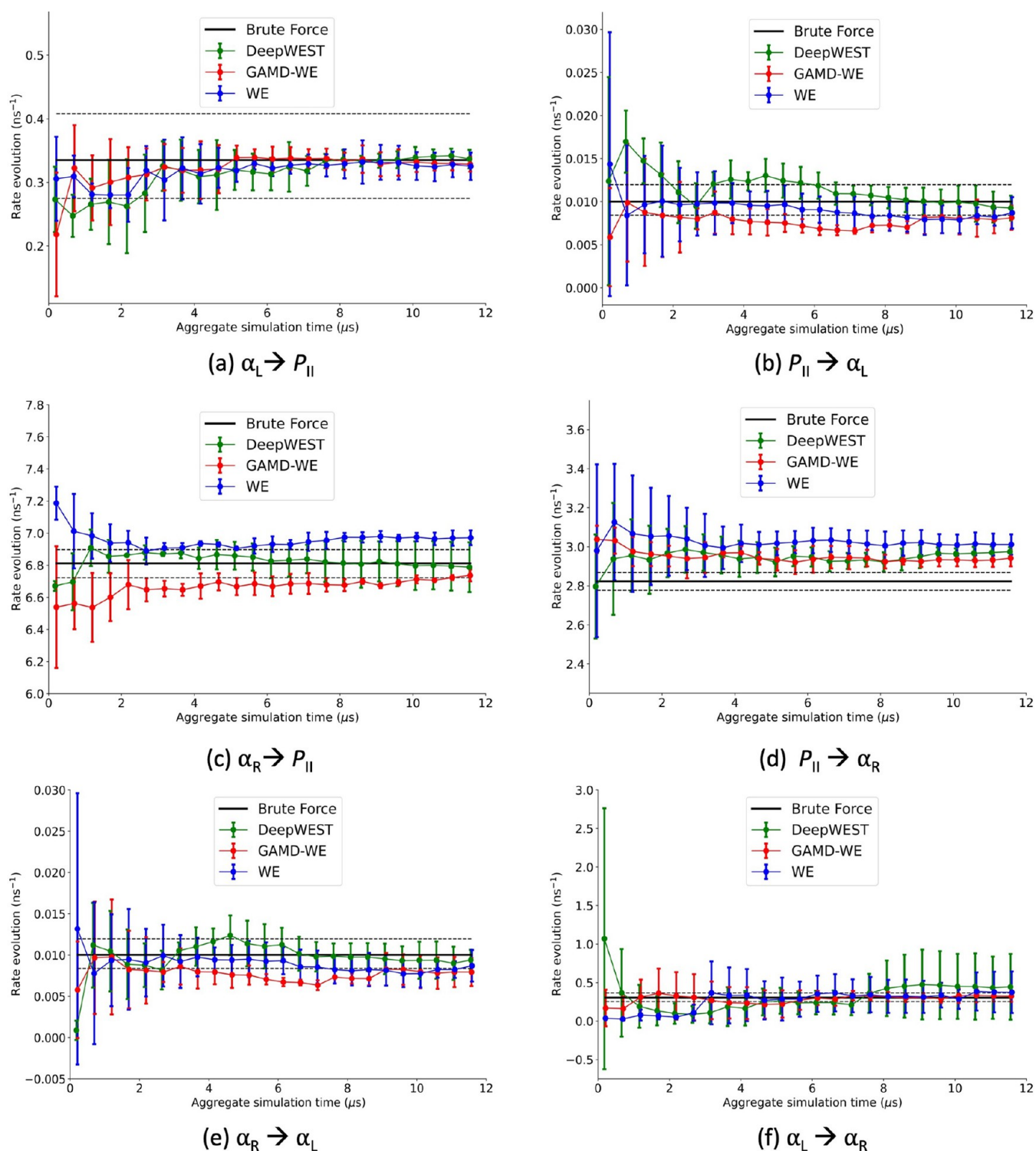


**Figure 6.** Evolution of rate constants over aggregate simulation time for the brute-force simulation (black), WE simulations (red), the GAMD-WE approach (blue), and the DeepWEST approach (green). For the WE, GaMD-WE, and DeepWEST methods, the error bars represent 95% confidence intervals obtained from the standard deviations of three independent runs.

potentials, and starting conformations were selected from the GaMD run that had the largest PES coverage. It was then followed by 39.50  $\mu\text{s}$  of WE simulations, totaling a simulation time of 120  $\mu\text{s}$  averaged over three independent runs of 40  $\mu\text{s}$  each. Likewise, for the DeepWEST approach, an unbiased MD simulation of 100 ns was run, followed by 39.90  $\mu\text{s}$  of WE simulation, totaling a simulation time of 120  $\mu\text{s}$  averaged over

three independent runs of 40  $\mu\text{s}$  each. Figure 8 demonstrates the ability of the deep-learned kinetic modeling approach to cluster the MSMs for chignolin. Initial conformations were selected from these metastable states for WE simulations. Figure 9a,b presents the average free energy profiles of chignolin from the WE and hybrid GaMD-WE approaches, respectively, while Figure 9c presents the free energy profile

**Table 3. Hyperparameters Used in VAMPNets for Chignolin**

hyperparameter	description	value
$\tau$	time lag between the two MD trajectory datasets	40 ps
batch size	number of samples in a batch for gradient descent	1000
train ratio	percentage of trajectory points used for training	0.9
network depth	number of hidden layers in the network	6
layer width	width of the hidden layer	100
learning rate	learning rate used for the ADAM optimizer	$1 \times 10^{-4}$
output size	number of metastable states as an output	3
$n_{\text{epochs}}$	number of iterations over the training set	100
$\epsilon$	threshold for eigenvalues	$1 \times 10^{-5}$

from the DeepWEST approach. Figure 10 demonstrates the average free energy profiles of chignolin from three separate runs of WE, GaMD-WE, and DeepWEST simulations at different stages of the simulations. The PES coverages for chignolin from the three approaches are comparable, demonstrating that the DeepWEST method can sample the thermodynamics of the system accurately.

To assess the performance of the DeepWEST approach with respect to WE and the hybrid GaMD-WE approach, we estimated the convergence of rate constants between metastable states, especially defined within folded and unfolded regions of chignolin (Table 4). The two intermediate regions,  $I_1$  and  $I_2$ , are separated apart in the PES, and convergence of rate constants between these regions is difficult to achieve. Figure 11c demonstrates faster and more accurate convergence of the DeepWEST approach compared to the WE and GaMD-WE approaches for the transition from  $I_1$  to  $I_2$ . However, the GaMD-WE method outperformed the DeepWEST method in estimating the rate constant for the transition from  $I_2$  to  $I_1$  (Figure 11d). The DeepWEST method showed faster convergence and greater accuracy in estimating the rate constants between  $I_2$  and the folded state (Figure 11e,f). Faster convergence for the DeepWEST method was also observed for the rate constant from the folded state to the unfolded state (Figure 11a). However, the GaMD-WE and DeepWEST methods equally outperformed the WE method in estimating the rate constant in the transition from the unfolded state to the folded state (Figure 11b). In conclusion, for all the cases, both the hybrid methods, especially the DeepWEST method, outperformed the WE method in achieving faster

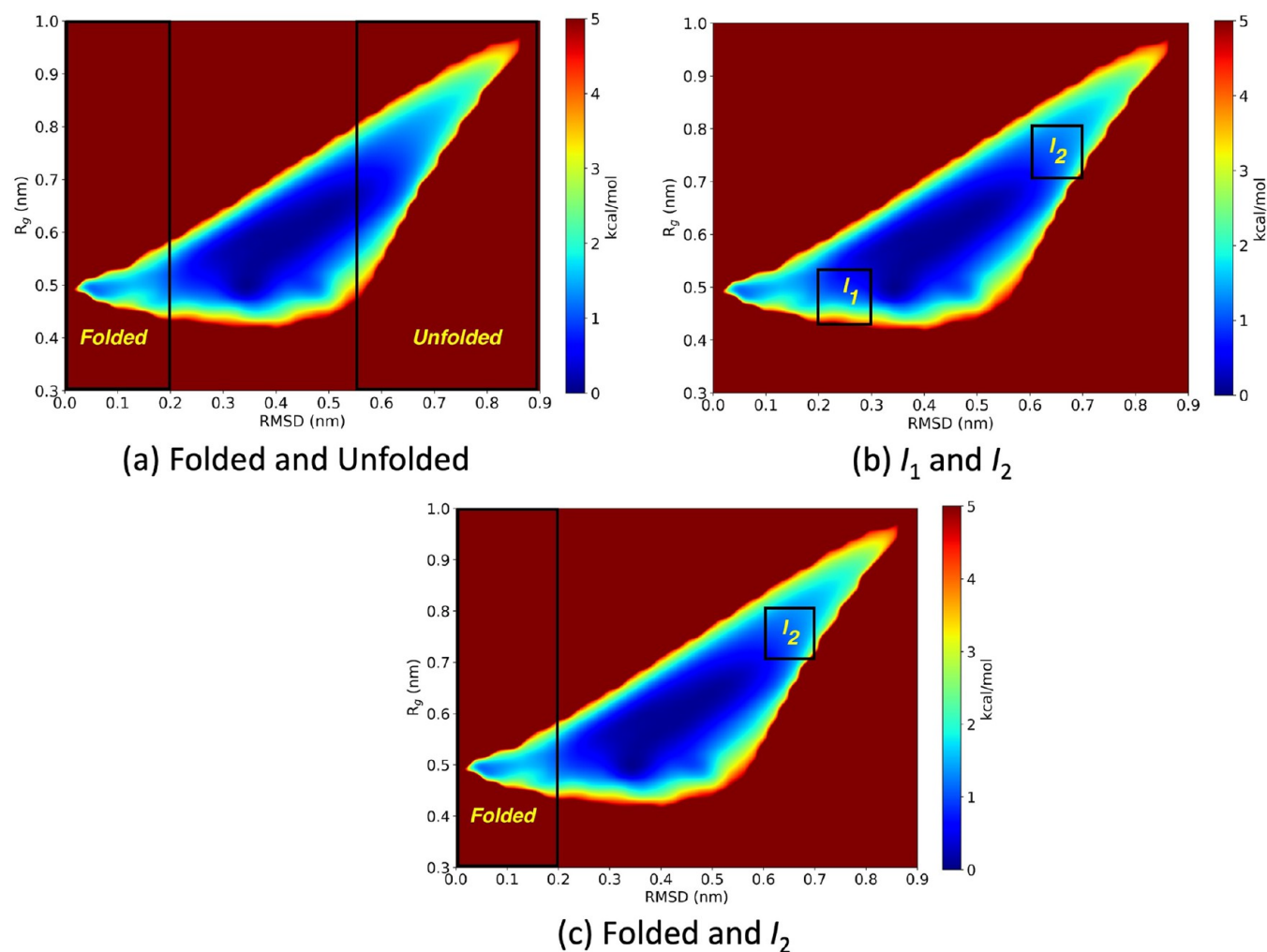


**Figure 7.** Average free energy profiles of chignolin from three separate 40  $\mu\text{s}$  runs of DeepWEST simulations. Rate constants to be calculated between the following regions of interest in chignolin: (a) folded  $\Leftrightarrow$  unfolded; (b)  $I_1 \Leftrightarrow I_2$ ; (c) folded  $\Leftrightarrow I_2$ .

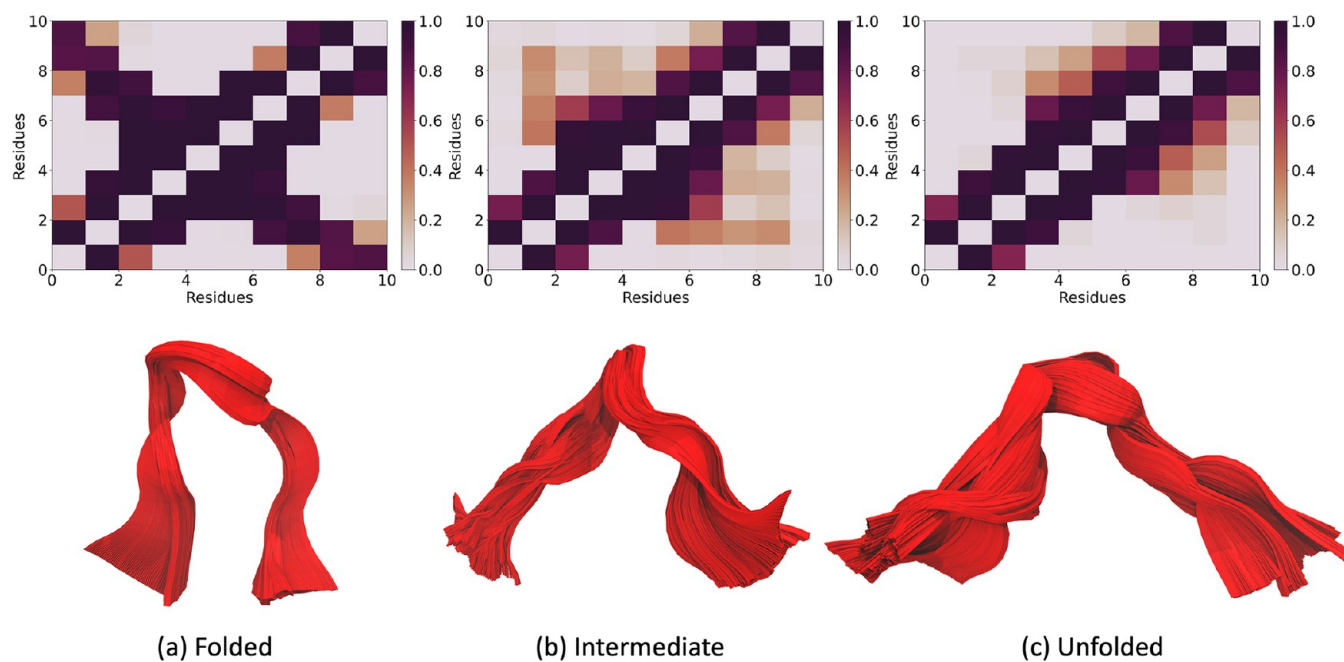


**Figure 8.** Three metastable states of chignolin as an output of VAMPNets. The upper panels show the mean contact maps for the metastable states, and the lower panels show the 3D representations of the states.

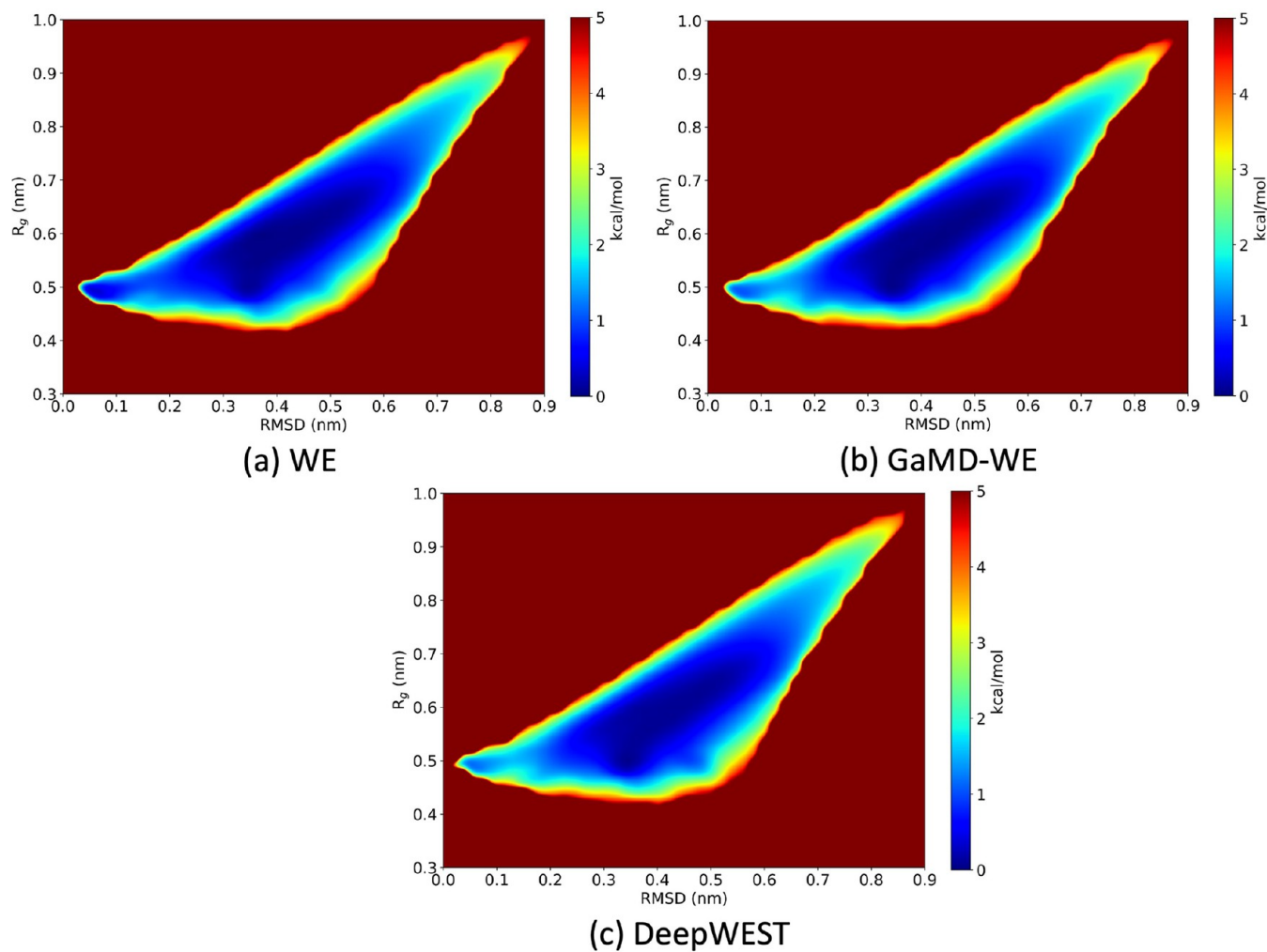


**Figure 9.** Average free energy profiles of chignolin from three separate 40  $\mu$ s runs of (a) WE, (b) GaMD-WE, and (c) DeepWEST simulations.



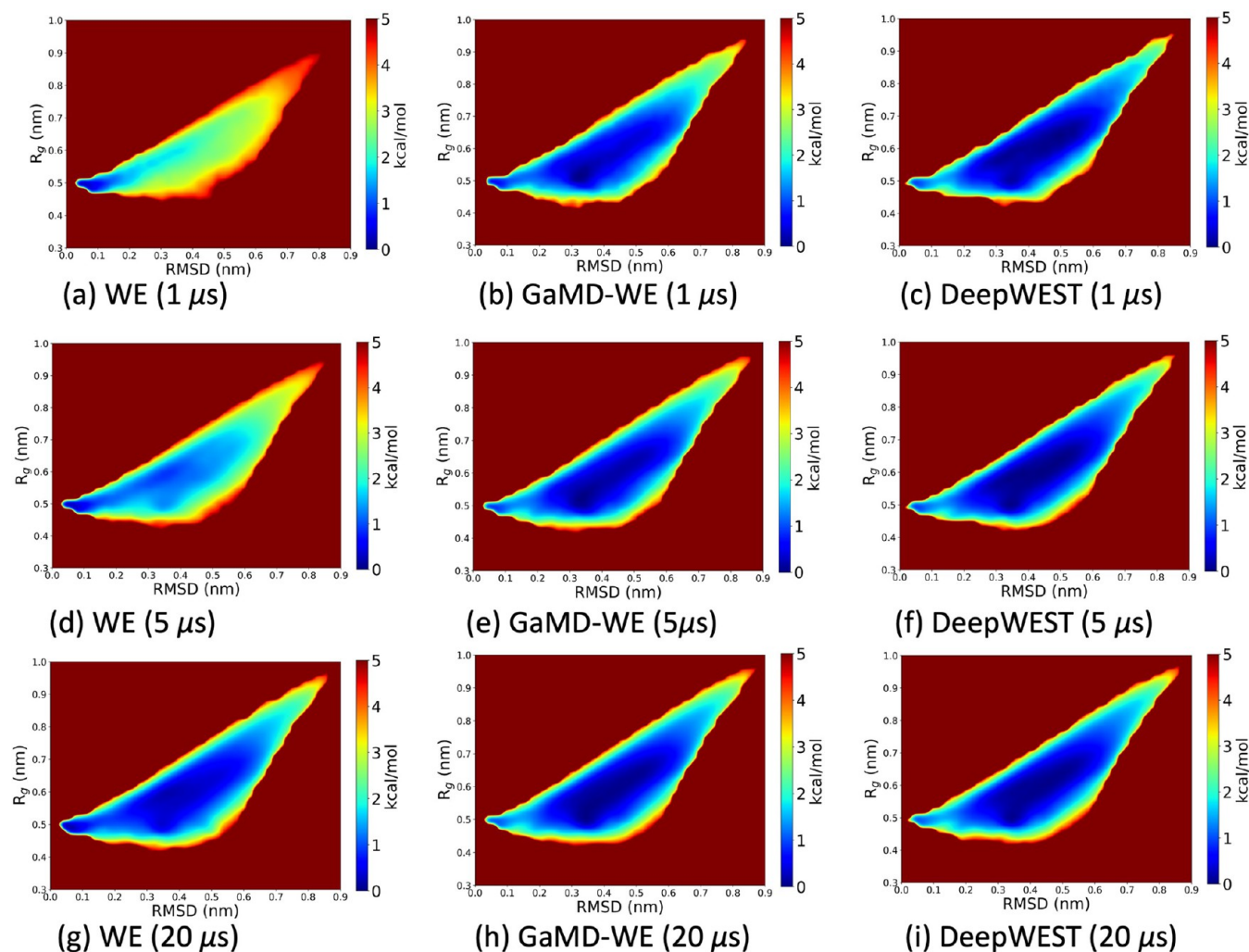


**Figure 10.** Average free energy profiles of chignolin from three separate runs of WE, GaMD-WE, and DeepWEST simulations at different stages of the simulations.

**Table 4.** Rate Constants (in  $\text{ns}^{-1}$ ) between Different Metastable States for Chignolin Obtained after 40  $\mu\text{s}$  of Aggregate Simulation Time

transition	brute-force <sup>a</sup>	WE <sup>b</sup>	GaMD-WE <sup>b</sup>	DeepWEST <sup>b</sup>
folded $\rightarrow$ unfolded	1.016 [0.983, 1.05]	$0.873 \pm 0.036$	$1.044 \pm 0.017$	$0.998 \pm 0.049$
unfolded $\rightarrow$ folded	0.144 [0.137, 0.15]	$0.159 \pm 0.002$	$0.148 \pm 0.003$	$0.149 \pm 0.013$
$I_1 \rightarrow I_2$	0.513 [0.501, 0.526]	$0.515 \pm 0.009$	$0.509 \pm 0.017$	$0.513 \pm 0.018$
$I_2 \rightarrow I_1$	0.316 [0.307, 0.325]	$0.327 \pm 0.012$	$0.325 \pm 0.015$	$0.324 \pm 0.007$
$I_2 \rightarrow$ folded	0.134 [0.127, 0.14]	$0.145 \pm 0.003$	$0.135 \pm 0.005$	$0.136 \pm 0.011$
folded $\rightarrow I_2$	0.519 [0.502, 0.536]	$0.49 \pm 0.009$	$0.506 \pm 0.016$	$0.511 \pm 0.015$

<sup>a</sup>In the case of brute-force simulation, the first value indicates the average rate constant, and the values within the brackets indicate the 95% confidence interval computed using Bayesian bootstrapping. <sup>b</sup>For the WE, GaMD-WE, and DeepWEST methods, the error bars represent 95% confidence intervals obtained from the standard deviations of three independent runs.

convergence and accuracy of rate constants between the metastable regions of interest.

**3.3. NTL9.** To further test the capabilities of the DeepWEST method for a higher-dimensional problem, we chose the N-terminal domain of ribosomal protein L9 (NTL9). The NTL9 protein is a 627-atom system consisting of 39 amino acid residues (Figure 1c) that has a folding time of  $\sim 1.5$  ms.<sup>100</sup> Initial coordinates for the unfolded NTL9 protein were obtained from [https://github.com/westpa/westpa2\\_tutorials/blob/main/tutorial-3.3/istates/ntl9.pdb](https://github.com/westpa/westpa2_tutorials/blob/main/tutorial-3.3/istates/ntl9.pdb). The system was then subjected to GB implicit solvation using the model II

radii.<sup>97–99</sup> The AMBER ff19SB force field was used to prepare the system for MD simulations.<sup>101</sup> The NTL9 protein was then subjected to 10  $\mu\text{s}$  of constant-volume unbiased MD simulation with a collision frequency of  $1 \text{ ps}^{-1}$ , employing a Langevin thermostat at a constant temperature of 300 K. To follow the folding and unfolding behavior of the NTL9 system, internal coordinates were chosen as a network input. Nearest-neighbor heavy-atom distances between all nonredundant residues separated by two or more residues served as the network input, resulting in 666 nodes. MD trajectories were trained using VAMP neural networks with a time lag of 60 ns, a

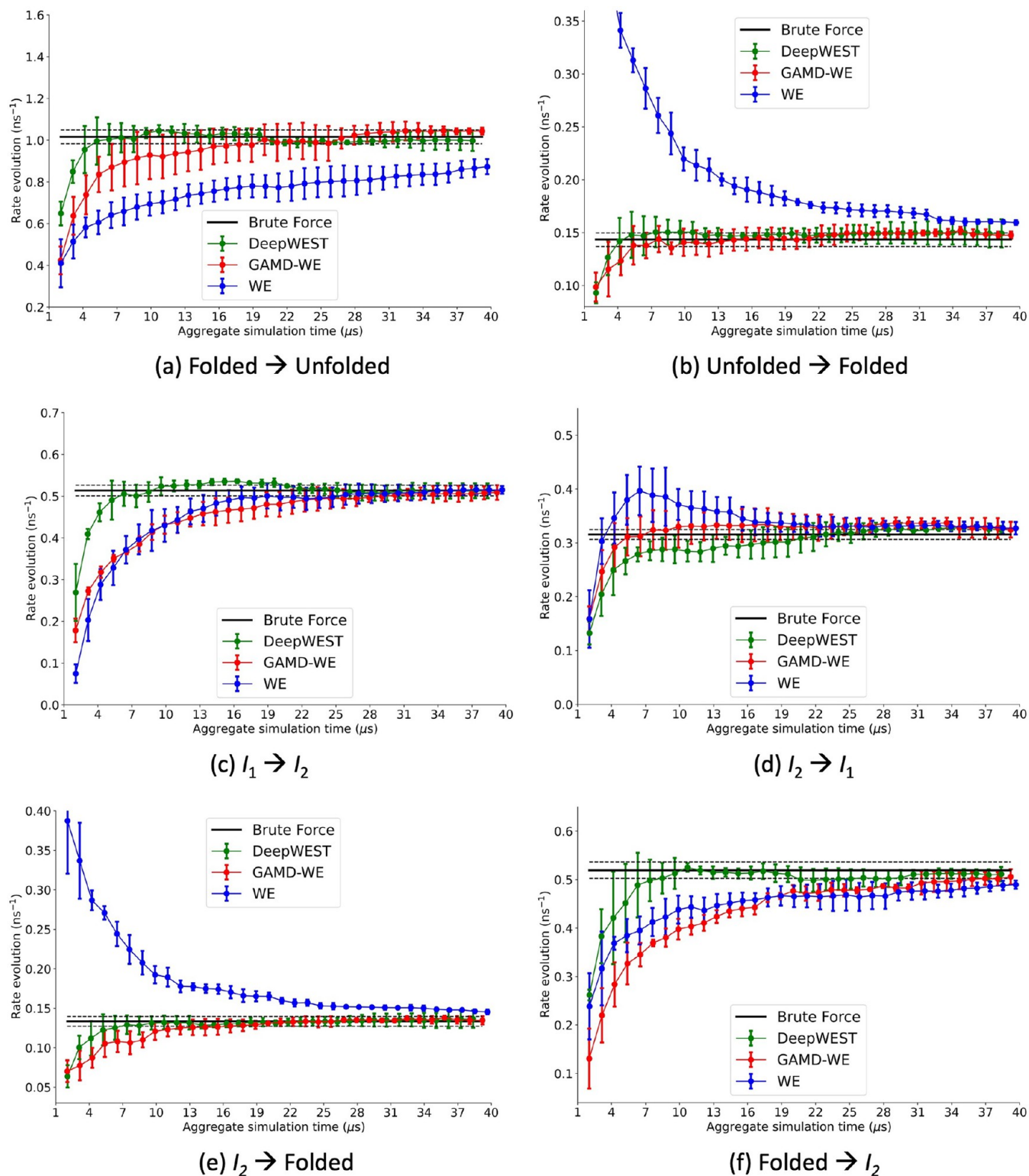


**Figure 11.** Evolution of rate constants over aggregate simulation time for the brute-force simulation (black), WE simulations (red), the GaMD-WE approach (blue), and the DeepWEST approach (green). For the WE, GaMD-WE, and DeepWEST methods, the error bars represent 95% confidence intervals obtained from the standard deviations of three independent runs.

training ratio of 0.9, and a batch size of 1000 that learned discretization in three metastable states by performing a hierarchical decomposition of the state space (Figure 12). Starting structures were selected from the metastable states as per the DeepWEST protocol followed by the WE simulation of 90 μs with a resampling time,  $\tau$ , of 40 ps. Therefore, the total

simulation time for the DeepWEST method was 120 μs. CVs for WE simulations were set to be mass-weighted RMSD and mass-weighted  $R_g$ , respectively. Both CVs were evenly spaced in bins of 0.05 nm in the range [0 nm, 2 nm]. The target number of walkers per bin,  $n_w$ , was set to 8 for the WE simulation. Similarly, the conventional WE simulation was run

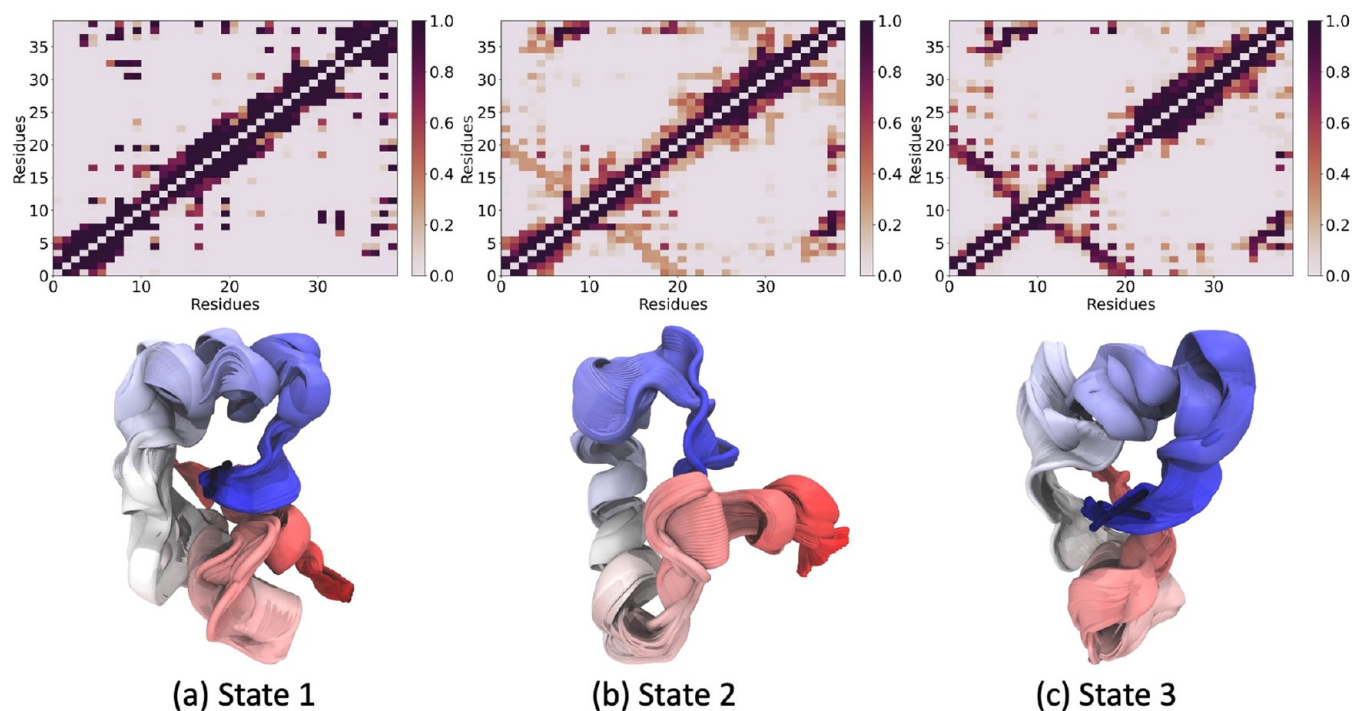


**Figure 12.** Three metastable states of the NTL9 system as an output of VAMPNets. The upper panels show the mean contact maps for the metastable states, and the lower panels show the 3D representations of the states.

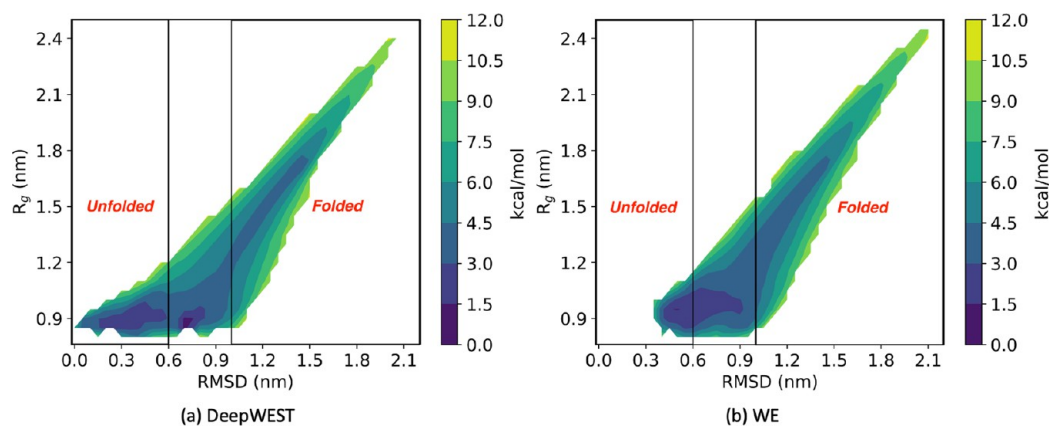


**Figure 13.** Average free energy profiles of NTL9 from 100  $\mu$ s runs of (a) DeepWEST and (b) WE simulations.

for 130  $\mu$ s with the same parameters (i.e., resampling time, CVs, and binning parameters) as described previously for the DeepWEST simulation. The WE simulations were initiated from the unfolded state to the folded state, with the CVs set to be the mass-weighted RMSD and mass-weighted  $R_g$ , respectively. Since the reference structure for computing the RMSD is the initial unfolded state, the RMSD is expected to increase during the simulation as the system folds. The unfolded region is defined as  $\text{RMSD} \leq 0.60$  nm, while the folded region is defined as  $\text{RMSD} \geq 1.0$  nm.

For the same amount of simulation time, i.e., 130  $\mu$ s, the DeepWEST method proved to be more effective than the conventional WE approach in covering the free energy landscape of a more complex protein, i.e., the NTL9 system. Figure 13a,b present the free energy landscapes for the NTL9 system for the DeepWEST and conventional WE methods, respectively, where the lowest-energy state was set to zero. It is evident from Figure 13a that the DeepWEST approach is more

effective than the conventional WE approach in exploring other metastable states in the NTL9 system, particularly in the unfolded region. The rate constants between the unfolded and folded states were not measured, but we expect the DeepWEST method to outperform the conventional WE method in kinetic rate measurements.

#### 4. DISCUSSION

The WE method predominantly depends on appropriate CVs to sample the system. In most cases, the best choice of CVs is unknown. In cases where CVs cannot sufficiently describe the system's dynamics, hybrid approaches and most enhanced sampling CV-free approaches may generate a well-sampled initial configurational space.<sup>26,51,102–105</sup> Initial sampling of the PES has a significant impact on the accuracy and convergence of WE. Our previously developed hybrid GaMD-WE method addresses the concern of substantial initial sampling, but reweighing is an additional concern associated with it. To



obtain the correct PES of the system, GaMD resorts to reweighing, and a substantial amount of energetic noise is introduced with an increase in the system size. In that case, GaMD needs to be run for a longer time scale for varying degrees of boost potentials, increasing the overall computational cost drastically. As demonstrated through previous examples, the newly developed DeepWEST approach is a powerful method that obtains both the kinetics and thermodynamics of the system. Compared to our earlier developed hybrid approach, it is a hassle-free method for enhanced sampling prior to running WE simulations. First, DeepWEST eliminates the process of running various accelerated MD simulations with varying degrees of boost potentials. Second, it also eliminates the process of PES reweighing to uncover the original energy landscape by running unbiased MD simulations. Most importantly, deep neural architectures learn the clustering of metastable states from short MD trajectories and can be further processed to extract starting conformations for WE simulations. Both methods involved in the DeepWEST approach add no statistical bias to the system, and thereby, kinetics and thermodynamics obtained from this approach are exact. However, a longer MD simulation time may be required to discretize metastable states as the system size increases to provide statistically relevant starting conformations for WE simulations. Recent improvements in the WE method have been made to achieve faster kinetics.<sup>55,104</sup> Even more accurate and faster kinetics and thermodynamic sampling could be achieved if DeepWEST were to be combined with these improvements in WE.

Currently, we have shown the DeepWEST method to work on simpler systems, i.e., alanine dipeptide in explicit solvation and chignolin in implicit solvation. We have also shown greater free energy landscape coverage for the NTL9 protein for the DeepWEST method against the conventional WE method. However, extending this method to more complex biological systems comes with challenges. Deep neural networks learn feature transformations and cluster trajectories based on input CVs. The network architecture for such systems primarily depends on the choice of time lag and the number of metastable states we want to cluster. Identifying the slowest processes in complex systems comes with the choice of accurate CVs, which in most cases is unknown. However, recent developments in enhanced MD sampling and MSM approaches would be worth considering. Implementing multiensemble Markov models (MEMMs) that conduct large ensembles of even shorter simulations and further accelerate trajectories by adding boosted potentials through various accelerated enhanced sampling methods in DeepWEST could aid the clustering of complex proteins.<sup>58,106</sup> Implementation of hydrogen-mass repartitioning (HMR) for solvated systems to accelerate the dynamics would prove indispensable in faster learning of metastable states.<sup>27</sup>

## 5. CONCLUSION

A hybrid approach for faster learning of kinetics combining deep learning of MD trajectories with WE simulations is presented here. It employs a deep learning architecture to sample statistically relevant conformations representative of the rare events from short MD simulation trajectories. The method is tested on three different model systems, namely, alanine dipeptide with explicit solvation, chignolin with implicit solvation, and the NTL9 protein with implicit

solvation. Our method significantly outperforms the WE and GaMD-WE approaches for the chignolin model system and is comparable in performance for the alanine dipeptide system. Because of its reduced simulation time and slighter sophistication compared to the GaMD-WE approach, DeepWEST allows for fast estimation of kinetics with enhanced coverage. We have also developed an end-to-end package, DeepWEST, that automates the entire process of running MD trajectories, extracting statistically relevant conformations using VAMP theory and neural networks, and preparing the WE simulation. The DeepWEST package is available at <https://github.com/anandojha/DeepWEST>. In conclusion, we have demonstrated a proof of concept of a hybrid data-driven approach that can be incorporated into the WE approach to obtain improved results with significantly less time and complexities.

## AUTHOR INFORMATION

### Corresponding Author

Rommie E. Amaro – Department of Chemistry, University of California San Diego, La Jolla, California 92093, United States; [orcid.org/0000-0002-9275-9553](https://orcid.org/0000-0002-9275-9553); Email: [ramaro@ucsd.edu](mailto:ramaro@ucsd.edu)

### Authors

Anupam Anand Ojha – Department of Chemistry, University of California San Diego, La Jolla, California 92093, United States; [orcid.org/0000-0001-6588-3092](https://orcid.org/0000-0001-6588-3092)

Saumya Thakur – Department of Chemistry, Indian Institute of Technology Bombay, Mumbai, Maharashtra 400076, India

Surl-Hee Ahn – Department of Chemical Engineering, University of California Davis, Davis, California 95616, United States; [orcid.org/0000-0002-3422-805X](https://orcid.org/0000-0002-3422-805X)

Complete contact information is available at: <https://pubs.acs.org/10.1021/acs.jctc.2c00282>

### Notes

The authors declare no competing financial interest.

## ACKNOWLEDGMENTS

A.A.O. acknowledges support through a Molecular Sciences Software Institute (MolSSI) Fellowship under NSF Grant OAC-1547580. R.E.A. acknowledges support from NSF Extreme Science and Engineering Discovery Environment (XSEDE) CHE060063 and NIH GM132826. All simulations were performed using the Triton Shared Computing Cluster (TSCC) and Expanse at the San Diego Supercomputing Center (SDSC). The latter allocation was supported by NSF XSEDE CHE060063 to R.E.A.

## REFERENCES

- (1) Durrant, J. D.; McCammon, J. A. Molecular dynamics simulations and drug discovery. *BMC Biol.* **2011**, *9*, 71.
- (2) Karplus, M.; Petsko, G. A. Molecular dynamics simulations in biology. *Nature* **1990**, *347*, 631–639.
- (3) Karplus, M.; McCammon, J. A. Molecular dynamics simulations of biomolecules. *Nat. Struct. Biol.* **2002**, *9*, 646–652.
- (4) Wood, W. W.; Erpenbeck, J. J. Molecular dynamics and Monte Carlo calculations in statistical mechanics. *Annu. Rev. Phys. Chem.* **1976**, *27*, 319–348.
- (5) Wereszczynski, J.; McCammon, J. A. Statistical mechanics and molecular dynamics in evaluating thermodynamic properties of biomolecular recognition. *Q. Rev. Biophys.* **2012**, *45*, 1–25.

- (6) Zheng, Q.; Chu, W.; Zhao, C.; Zhang, L.; Guo, H.; Wang, Y.; Jiang, X.; Zhao, J. Ab initio nonadiabatic molecular dynamics investigations on the excited carriers in condensed matter systems. *Wiley Interdiscip. Rev.: Comput. Mol. Sci.* **2019**, *9*, No. e1411.
- (7) Smith, B.; Akimov, A. V. Modeling nonadiabatic dynamics in condensed matter materials: some recent advances and applications. *J. Phys.: Condens. Matter* **2020**, *32*, 073001.
- (8) Steinhäuser, M. O.; Hiermaier, S. A review of computational methods in materials science: examples from shock-wave and polymer physics. *Int. J. Mol. Sci.* **2009**, *10*, S135–S216.
- (9) *Molecular Dynamics Simulations of Disordered Materials*; Massobrio, C., Du, J., Bernasconi, M., Salmon, P. S., Eds.; Springer International Publishing: Cham, Switzerland, 2015.
- (10) Akimov, A. V.; Prezhdo, O. V. The PYXAID program for non-adiabatic molecular dynamics in condensed matter systems. *J. Chem. Theory Comput.* **2013**, *9*, 4959–4972.
- (11) Piggot, T. J.; Holdbrook, D. A.; Khalid, S. Conformational dynamics and membrane interactions of the E. coli outer membrane protein FecA: a molecular dynamics simulation study. *Biochim. Biophys. Acta, Biomembr.* **2013**, *1828*, 284–293.
- (12) Lindahl, E.; Sansom, M. S. Membrane proteins: molecular dynamics simulations. *Curr. Opin. Struct. Biol.* **2008**, *18*, 425–431.
- (13) Swope, W. C.; Pitera, J. W.; Suits, F.; Pitman, M.; Eleftheriou, M.; Fitch, B. G.; Germain, R. S.; Rayshubski, A.; Ward, T. C.; Zhestkov, Y.; Zhou, R. Describing protein folding kinetics by molecular dynamics simulations. 2. Example applications to alanine dipeptide and a  $\beta$ -hairpin peptide. *J. Phys. Chem. B* **2004**, *108*, 6582–6594.
- (14) Chodera, J. D.; Swope, W. C.; Pitera, J. W.; Dill, K. A. Long-time protein folding dynamics from short-time molecular dynamics simulations. *Multiscale Model. Simul.* **2006**, *5*, 1214–1226.
- (15) Cui, Q.; Sulea, T.; Schrag, J. D.; Munger, C.; Hung, M.-N.; Naïm, M.; Cygler, M.; Purisima, E. O. Molecular dynamics—Solvated interaction energy studies of protein–protein interactions: The MP1–p14 scaffolding complex. *J. Mol. Biol.* **2008**, *379*, 787–802.
- (16) Rakers, C.; Bermudez, M.; Keller, B. G.; Mortier, J.; Wolber, G. Computational close up on protein–protein interactions: how to unravel the invisible using molecular dynamics simulations? *Wiley Interdiscip. Rev.: Comput. Mol. Sci.* **2015**, *5*, 345–359.
- (17) De Vivo, M.; Masetti, M.; Bottogoni, G.; Cavalli, A. Role of molecular dynamics and related methods in drug discovery. *J. Med. Chem.* **2016**, *59*, 4035–4061.
- (18) Liu, K.; Watanabe, E.; Kokubo, H. Exploring the stability of ligand binding modes to proteins by molecular dynamics simulations. *J. Comput.-Aided Mol. Des.* **2017**, *31*, 201–211.
- (19) Jorgensen, W. L.; Jensen, K. P.; Alexandrova, A. N. Polarization effects for hydrogen-bonded complexes of substituted phenols with water and chloride ion. *J. Chem. Theory Comput.* **2007**, *3*, 1987–1992.
- (20) Tkatchenko, A.; DiStasio, R. A., Jr; Car, R.; Scheffler, M. Accurate and efficient method for many-body van der Waals interactions. *Phys. Rev. Lett.* **2012**, *108*, 236402.
- (21) Tkatchenko, A.; Scheffler, M. Accurate molecular van der Waals interactions from ground-state electron density and free-atom reference data. *Phys. Rev. Lett.* **2009**, *102*, 073005.
- (22) Hartmann, C.; Banisch, R.; Sarich, M.; Badowski, T.; Schütte, C. Characterization of rare events in molecular dynamics. *Entropy* **2014**, *16*, 350–376.
- (23) Anderson, J. B. Predicting rare events in molecular dynamics. *Adv. Chem. Phys.* **2007**, *91*, 381–432.
- (24) Passerone, D.; Parrinello, M. Action-derived molecular dynamics in the study of rare events. *Phys. Rev. Lett.* **2001**, *87*, 108302.
- (25) Zwier, M. C.; Chong, L. T. Reaching biological timescales with all-atom molecular dynamics simulations. *Curr. Opin. Pharmacol.* **2010**, *10*, 745–752.
- (26) Yang, Y. I.; Shao, Q.; Zhang, J.; Yang, L.; Gao, Y. Q. Enhanced sampling in molecular dynamics. *J. Chem. Phys.* **2019**, *151*, 070902.
- (27) Hopkins, C. W.; Le Grand, S.; Walker, R. C.; Roitberg, A. E. Long-time-step molecular dynamics through hydrogen mass repartitioning. *J. Chem. Theory Comput.* **2015**, *11*, 1864–1874.
- (28) Tuckerman, M. E.; Martyna, G. J.; Berne, B. J. Molecular dynamics algorithm for condensed systems with multiple time scales. *J. Chem. Phys.* **1990**, *93*, 1287–1291.
- (29) Feenstra, K. A.; Hess, B.; Berendsen, H. J. Improving efficiency of large time-scale molecular dynamics simulations of hydrogen-rich systems. *Journal of computational chemistry* **1999**, *20*, 786–798.
- (30) Laio, A.; Gervasio, F. L. Metadynamics: a method to simulate rare events and reconstruct the free energy in biophysics, chemistry and material science. *Rep. Prog. Phys.* **2008**, *71*, 126601.
- (31) Bussi, G.; Laio, A.; Parrinello, M. Equilibrium free energies from nonequilibrium metadynamics. *Phys. Rev. Lett.* **2006**, *96*, 090601.
- (32) Valsson, O.; Parrinello, M. Variational approach to enhanced sampling and free energy calculations. *Phys. Rev. Lett.* **2014**, *113*, 090601.
- (33) Chodera, J. D.; Noé, F. Markov state models of biomolecular conformational dynamics. *Curr. Opin. Struct. Biol.* **2014**, *25*, 135–144.
- (34) Husic, B. E.; Pande, V. S. Markov state models: From an art to a science. *J. Am. Chem. Soc.* **2018**, *140*, 2386–2396.
- (35) Sugita, Y.; Okamoto, Y. Replica-exchange molecular dynamics method for protein folding. *Chem. Phys. Lett.* **1999**, *314*, 141–151.
- (36) Yang, L.; Gao, Y. Q. A selective integrated tempering method. *J. Chem. Phys.* **2009**, *131*, 214109.
- (37) Miao, Y.; McCammon, J. A. *Annu. Rep. Computat. Chem.* **2017**, *13*, 231–278.
- (38) Miao, Y. Acceleration of biomolecular kinetics in Gaussian accelerated molecular dynamics. *J. Chem. Phys.* **2018**, *149*, 072308.
- (39) Stelzl, L. S.; Hummer, G. Kinetics from replica exchange molecular dynamics simulations. *J. Chem. Theory Comput.* **2017**, *13*, 3927–3935.
- (40) Buchete, N.-V.; Hummer, G. Peptide folding kinetics from replica exchange molecular dynamics. *Phys. Rev. E* **2008**, *77*, 030902.
- (41) Tiwary, P.; Parrinello, M. From metadynamics to dynamics. *Phys. Rev. Lett.* **2013**, *111*, 230602.
- (42) Yang, L.; Liu, C.-W.; Shao, Q.; Zhang, J.; Gao, Y. Q. From thermodynamics to kinetics: enhanced sampling of rare events. *Acc. Chem. Res.* **2015**, *48*, 947–955.
- (43) Zuckerman, D. M.; Chong, L. T. Weighted ensemble simulation: review of methodology, applications, and software. *Annu. Rev. Biophys.* **2017**, *46*, 43–57.
- (44) Votapka, L. W.; Stokely, A. M.; Ojha, A. A.; Amaro, R. E. SEEKRR2: Versatile Multiscale Milestoning Utilizing the OpenMM Molecular Dynamics Engine. *J. Chem. Inf. Model.* **2022**, *62*, 3253–3262.
- (45) Jagger, B. R.; Ojha, A. A.; Amaro, R. E. Predicting ligand binding kinetics using a Markovian milestoning with voronoi tessellations multiscale approach. *J. Chem. Theory Comput.* **2020**, *16*, 5348–5357.
- (46) Vanden-Eijnden, E.; Venturoli, M. Markovian milestoning with Voronoi tessellations. *J. Chem. Phys.* **2009**, *130*, 194101.
- (47) Cérou, F.; Guyader, A. Adaptive multilevel splitting for rare event analysis. *Stochastic Anal. Appl.* **2007**, *25*, 417–443.
- (48) L'Ecuyer, P.; Demers, V.; Tuffin, B. Splitting for rare-event simulation. In *Proceedings of the 2006 Winter Simulation Conference*, 2006; pp 137–148.
- (49) Cérou, F.; Del Moral, P.; Furon, T.; Guyader, A. Sequential Monte Carlo for rare event estimation. *Stat. Comput.* **2012**, *22*, 795–808.
- (50) Van Erp, T. S.; Bolhuis, P. G. Elaborating transition interface sampling methods. *J. Comput. Phys.* **2005**, *205*, 157–181.
- (51) Ahn, S.-H.; Ojha, A. A.; Amaro, R. E.; McCammon, J. A. Gaussian-Accelerated Molecular Dynamics with the Weighted Ensemble Method: A Hybrid Method Improves Thermodynamic and Kinetic Sampling. *J. Chem. Theory Comput.* **2021**, *17*, 7938–7951.
- (52) Wu, H.; Noé, F. Variational approach for learning Markov processes from time series data. *J. Nonlinear Sci.* **2020**, *30*, 23–66.
- (53) LeCun, Y.; Bengio, Y.; Hinton, G. Deep learning. *Nature* **2015**, *521*, 436–444.
- (54) Bacci, M.; Cafilisch, A.; Vitalis, A. On the removal of initial state bias from simulation data. *J. Chem. Phys.* **2019**, *150*, 104105.

- (55) Russo, J. D.; Zhang, S.; Leung, J. M.; Bogetti, A. T.; Thompson, J. P.; DeGrave, A. J.; Torrillo, P. A.; Pratt, A.; Wong, K. F.; Xia, J.; Copperman, J.; Adelman, J. L.; Zwier, M. C.; LeBard, D. N.; Zuckerman, D. M.; Chong, L. T. WESTPA 2.0: High-performance upgrades for weighted ensemble simulations and analysis of longer-timescale applications. *J. Chem. Theory Comput.* **2022**, *18*, 638–649.
- (56) Prinz, J.-H.; Wu, H.; Sarich, M.; Keller, B.; Senne, M.; Held, M.; Chodera, J. D.; Schütte, C.; Noé, F. Markov models of molecular kinetics: Generation and validation. *J. Chem. Phys.* **2011**, *134*, 174105.
- (57) Bowman, G. R.; Bolin, E. R.; Hart, K. M.; Maguire, B. C.; Marqusee, S. Discovery of multiple hidden allosteric sites by combining Markov state models and experiments. *Proc. Natl. Acad. Sci. U. S. A.* **2015**, *112*, 2734–2739.
- (58) Wu, H.; Paul, F.; Wehmeyer, C.; Noé, F. Multiensemble Markov models of molecular thermodynamics and kinetics. *Proc. Natl. Acad. Sci. U. S. A.* **2016**, *113*, E3221–E3230.
- (59) Schütte, C.; Fischer, A.; Huisinga, W.; Deuffhard, P. A direct approach to conformational dynamics based on hybrid Monte Carlo. *J. Comput. Phys.* **1999**, *151*, 146–168.
- (60) Schwantes, C. R.; Pande, V. S. Modeling molecular kinetics with tICA and the kernel trick. *J. Chem. Theory Comput.* **2015**, *11*, 600–608.
- (61) Boninsegna, L.; Gobbo, G.; Noé, F.; Clementi, C. Investigating molecular kinetics by variationally optimized diffusion maps. *J. Chem. Theory Comput.* **2015**, *11*, S947–S960.
- (62) Pérez-Hernández, G.; Paul, F.; Giorgino, T.; De Fabritiis, G.; Noé, F. Identification of slow molecular order parameters for Markov model construction. *J. Chem. Phys.* **2013**, *139*, 015102.
- (63) Noé, F.; Nuske, F. A variational approach to modeling slow processes in stochastic dynamical systems. *Multiscale Model. Simul.* **2013**, *11*, 635–655.
- (64) Williams, M. O.; Kevrekidis, I. G.; Rowley, C. W. A data-driven approximation of the koopman operator: Extending dynamic mode decomposition. *J. Nonlinear Sci.* **2015**, *25*, 1307–1346.
- (65) Korda, M.; Putinar, M.; Mezić, I. Data-driven spectral analysis of the Koopman operator. *Appl. Comput. Harmonic Anal.* **2020**, *48*, 599–629.
- (66) Korda, M.; Mezić, I. Linear predictors for nonlinear dynamical systems: Koopman operator meets model predictive control. *Automatica* **2018**, *93*, 149–160.
- (67) Mezić, I. Spectral properties of dynamical systems, model reduction and decompositions. *Nonlinear Dyn.* **2005**, *41*, 309–325.
- (68) Koopman, B. O. Hamiltonian systems and transformation in Hilbert space. *Proc. Natl. Acad. Sci. U. S. A.* **1931**, *17*, 315–318.
- (69) Mardt, A.; Pasquali, L.; Wu, H.; Noé, F. VAMPnets for deep learning of molecular kinetics. *Nat. Commun.* **2018**, *9*, 5.
- (70) Doerr, S.; Harvey, M.; Noé, F.; De Fabritiis, G. HTMD: high-throughput molecular dynamics for molecular discovery. *J. Chem. Theory Comput.* **2016**, *12*, 1845–1852.
- (71) Scherer, M. K.; Trendelkamp-Schroer, B.; Paul, F.; Pérez-Hernández, G.; Hoffmann, M.; Plattner, N.; Wehmeyer, C.; Prinz, J.-H.; Noé, F. PyEMMA 2: A software package for estimation, validation, and analysis of Markov models. *J. Chem. Theory Comput.* **2015**, *11*, S525–S542.
- (72) Harrigan, M. P.; Sultan, M. M.; Hernández, C. X.; Husic, B. E.; Eastman, P.; Schwantes, C. R.; Beauchamp, K. A.; McGibbon, R. T.; Pande, V. S. MSMBuilder: statistical models for biomolecular dynamics. *Biophys. J.* **2017**, *112*, 10–15.
- (73) McGibbon, R. T.; Beauchamp, K. A.; Harrigan, M. P.; Klein, C.; Swails, J. M.; Hernández, C. X.; Schwantes, C. R.; Wang, L.-P.; Lane, T. J.; Pande, V. S. MDTraj: a modern open library for the analysis of molecular dynamics trajectories. *Biophys. J.* **2015**, *109*, 1528–1532.
- (74) Schmid, P. J. Dynamic mode decomposition of numerical and experimental data. *J. Fluid. Mech.* **2010**, *656*, 5–28.
- (75) Wu, H.; Nüske, F.; Paul, F.; Klus, S.; Koltai, P.; Noé, F. Variational Koopman models: Slow collective variables and molecular kinetics from short off-equilibrium simulations. *J. Chem. Phys.* **2017**, *146*, 154104.
- (76) Molgedey, L.; Schuster, H. G. Separation of a mixture of independent signals using time delayed correlations. *Phys. Rev. Lett.* **1994**, *72*, 3634.
- (77) Chodera, J. D.; Singhal, N.; Pande, V. S.; Dill, K. A.; Swope, W. C. Automatic discovery of metastable states for the construction of Markov models of macromolecular conformational dynamics. *J. Chem. Phys.* **2007**, *126*, 155101.
- (78) Husic, B. E.; Pande, V. S. Ward clustering improves cross-validated Markov state models of protein folding. *J. Chem. Theory Comput.* **2017**, *13*, 963–967.
- (79) Kube, S.; Weber, M. A coarse graining method for the identification of transition rates between molecular conformations. *J. Chem. Phys.* **2007**, *126*, 024103.
- (80) Yao, Y.; Cui, R. Z.; Bowman, G. R.; Silva, D.-A.; Sun, J.; Huang, X. Hierarchical Nyström methods for constructing Markov state models for conformational dynamics. *J. Chem. Phys.* **2013**, *138*, 174106.
- (81) Huber, G. A.; Kim, S. Weighted-ensemble Brownian dynamics simulations for protein association reactions. *Biophys. J.* **1996**, *70*, 97–110.
- (82) Zhang, B. W.; Jasnow, D.; Zuckerman, D. M. The “weighted ensemble” path sampling method is statistically exact for a broad class of stochastic processes and binning procedures. *J. Chem. Phys.* **2010**, *132*, 054107.
- (83) Copperman, J.; Zuckerman, D. M. Accelerated estimation of long-timescale kinetics from weighted ensemble simulation via non-markovian “microbin” analysis. *J. Chem. Theory Comput.* **2020**, *16*, 6763–6775.
- (84) Donyapour, N.; Roussey, N. M.; Dickson, A. REVO: Resampling of ensembles by variation optimization. *J. Chem. Phys.* **2019**, *150*, 244112.
- (85) Aristoff, D. Analysis and optimization of weighted ensemble sampling. *ESAIM: Math. Modell. Numer. Anal.* **2018**, *52*, 1219–1238.
- (86) Zwier, M. C.; Adelman, J. L.; Kaus, J. W.; Pratt, A. J.; Wong, K. F.; Rego, N. B.; Suárez, E.; Lettieri, S.; Wang, D. W.; Grabe, M.; Zuckerman, D. M.; Chong, L. T. WESTPA: An interoperable, highly scalable software package for weighted ensemble simulation and analysis. *J. Chem. Theory Comput.* **2015**, *11*, 800–809.
- (87) Pearlman, D. A.; Case, D. A.; Caldwell, J. W.; Ross, W. S.; Cheatham, T. E., III; DeBolt, S.; Ferguson, D.; Seibel, G.; Kollman, P. AMBER, a package of computer programs for applying molecular mechanics, normal mode analysis, molecular dynamics and free energy calculations to simulate the structural and energetic properties of molecules. *Comput. Phys. Commun.* **1995**, *91*, 1–41.
- (88) Eastman, P.; Swails, J.; Chodera, J. D.; McGibbon, R. T.; Zhao, Y.; Beauchamp, K. A.; Wang, L.-P.; Simmonett, A. C.; Harrigan, M. P.; Stern, C. D.; Wiewiora, R. P.; Brooks, B. R.; Pande, V. S. OpenMM 7: Rapid development of high performance algorithms for molecular dynamics. *PLoS Comput. Biol.* **2017**, *13*, No. e1005659.
- (89) van der Spoel, D.; Lindahl, E. Brute-force molecular dynamics simulations of villin headpiece: comparison with NMR parameters. *J. Phys. Chem. B* **2003**, *107*, 11178–11187.
- (90) Mironov, V.; Alexeev, Y.; Mulligan, V. K.; Fedorov, D. G. A systematic study of minima in alanine dipeptide. *J. Comput. Chem.* **2019**, *40*, 297–309.
- (91) Rossky, P. J.; Karplus, M. Solvation. A molecular dynamics study of a dipeptide in water. *J. Am. Chem. Soc.* **1979**, *101*, 1913–1937.
- (92) Sinko, W.; Miao, Y.; de Oliveira, C. A. F.; McCammon, J. A. Population based reweighting of scaled molecular dynamics. *J. Phys. Chem. B* **2013**, *117*, 12759–12768.
- (93) Maier, J. A.; Martinez, C.; Kasavajhala, K.; Wickstrom, L.; Hauser, K. E.; Simmerling, C. ff14SB: improving the accuracy of protein side chain and backbone parameters from ff99SB. *J. Chem. Theory Comput.* **2015**, *11*, 3696–3713.
- (94) MacKerell, A. D., Jr.; Bashford, D.; Bellott, M.; Dunbrack, R. L., Jr.; Evanseck, J. D.; Field, M. J.; Fischer, S.; Gao, J.; Guo, H.; Ha, S.; Joseph-McCarthy, D.; Kuchnir, L.; Kuczera, K.; Lau, F. T. K.; Mattos, C.; Michnick, S.; Ngo, T.; Nguyen, D. T.; Prodhom, B.; Reiher, W. E.;



Roux, B.; Schlenkrich, M.; Smith, J. C.; Stote, R.; Straub, J.; Watanabe, M.; Wiórkiewicz-Kuczera, J.; Yin, D.; Karplus, M. All-atom empirical potential for molecular modeling and dynamics studies of proteins. *J. Phys. Chem. B* **1998**, *102*, 3586–3616.

(95) Honda, S.; Yamasaki, K.; Sawada, Y.; Morii, H. 10 residue folded peptide designed by segment statistics. *Structure* **2004**, *12*, 1507–1518.

(96) Satoh, D.; Shimizu, K.; Nakamura, S.; Terada, T. Folding free-energy landscape of a 10-residue mini-protein, chignolin. *FEBS Lett.* **2006**, *580*, 3422–3426.

(97) Feig, M.; Im, W.; Brooks, C. L., III. Implicit solvation based on generalized Born theory in different dielectric environments. *J. Chem. Phys.* **2004**, *120*, 903–911.

(98) Onufriev, A. V.; Case, D. A. Generalized Born implicit solvent models for biomolecules. *Annu. Rev. Biophys.* **2019**, *48*, 275–296.

(99) Onufriev, A.; Bashford, D.; Case, D. A. Exploring protein native states and large-scale conformational changes with a modified generalized born model. *Proteins: Struct., Funct., Bioinf.* **2004**, *55*, 383–394.

(100) Voelz, V. A.; Bowman, G. R.; Beauchamp, K.; Pande, V. S. Molecular simulation of ab initio protein folding for a millisecond folder NTL9 (1–39). *J. Am. Chem. Soc.* **2010**, *132*, 1526–1528.

(101) Tian, C.; Kasavajhala, K.; Belfon, K. A.; Raguette, L.; Huang, H.; Míguas, A. N.; Bickel, J.; Wang, Y.; Pincay, J.; Wu, Q.; Simmerling, C. ff19SB: Amino-acid-specific protein backbone parameters trained against quantum mechanics energy surfaces in solution. *J. Chem. Theory Comput.* **2020**, *16*, 528–552.

(102) Bussi, G.; Laio, A. Using metadynamics to explore complex free-energy landscapes. *Nat. Rev. Phys.* **2020**, *2*, 200–212.

(103) Fu, H.; Chen, H.; Wang, X.; Chai, H.; Shao, X.; Cai, W.; Chipot, C. Finding an optimal pathway on a multidimensional free-energy landscape. *J. Chem. Inf. Model.* **2020**, *60*, 5366–5374.

(104) Ray, D.; Stone, S. E.; Andricioaei, I. Markovian Weighted Ensemble Milestoning (M-WEM): Long-time Kinetics from Short Trajectories. *J. Chem. Theory Comput.* **2022**, *18*, 79–95.

(105) Miao, Y.; Bhattarai, A.; Wang, J. Ligand Gaussian accelerated molecular dynamics (LiGaMD): Characterization of ligand binding thermodynamics and kinetics. *J. Chem. Theory Comput.* **2020**, *16*, 5526–5547.

(106) Wu, H.; Mey, A. S. J. S.; Rosta, E.; Noé, F. Statistically optimal analysis of state-discretized trajectory data from multiple thermodynamic states. *J. Chem. Phys.* **2014**, *141*, 214106.

## Recommended by ACS

### Stochastic Approximation to MBAR and TRAM: Batchwise Free Energy Estimation

Maaïke M. Galama, Frank Noé, *et al.*

JANUARY 23, 2023

JOURNAL OF CHEMICAL THEORY AND COMPUTATION

READ 

### Skipping the Replica Exchange Ladder with Normalizing Flows

Michele Invernizzi, Frank Noé, *et al.*

DECEMBER 09, 2022

THE JOURNAL OF PHYSICAL CHEMISTRY LETTERS

READ 

### Re-Balancing Replica Exchange with Solute Tempering for Sampling Dynamic Protein Conformations

Yumeng Zhang, Jianhan Chen, *et al.*

FEBRUARY 15, 2023

JOURNAL OF CHEMICAL THEORY AND COMPUTATION

READ 

### Temporally Coherent Backmapping of Molecular Trajectories From Coarse-Grained to Atomistic Resolution

Kirill Shmilovich, Moritz Hoffmann, *et al.*

NOVEMBER 23, 2022

THE JOURNAL OF PHYSICAL CHEMISTRY A

READ 

Get More Suggestions >